NATIONAL ENERGY TECHNOLOGY LABORATORY

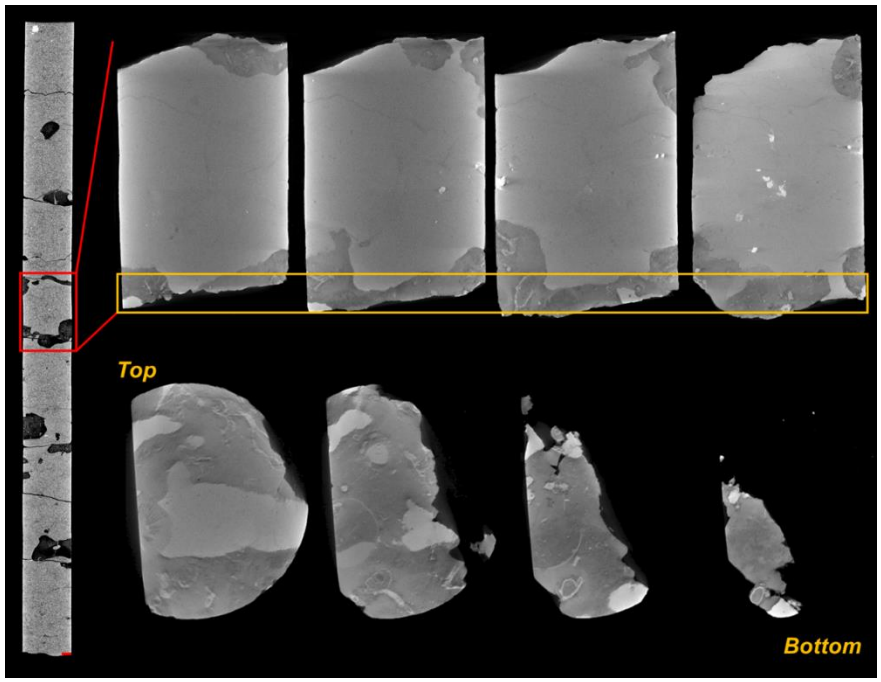

Computed Tomography Scanning and Geophysical Measurements of the CarbonSAFE Seal Integrity Wells in the Illinois Basin

20 March 2023

U.S. DEPARTMENT OF ENERGY | NATIONAL ENERGY TECHNOLOGY LABORATORY

Office of Fossil Energy and Carbon Management

DOE/NETL-2023/4323

Disclaimer

This project was funded by the U.S. Department of Energy, National Energy Technology Laboratory, in part, through a site support contract.

Cover Illustration: Left: Medical CT image from GM #2 from 6,200 to 6,205 ft, red scale bar indicates 2 cm; **Right, top:** Industrial CT image montage from 6,202 ft in the YZ orientation; **Right, bottom:** Industrial CT image montage from 6,202 ft in the XY orientation for the extent of the yellow box, highlighting a fossiliferous region of the scan.

Suggested Citation: Paronish, T.; Mitchell, N.; Brown, S.; Pohl, M.; Crandall, D.; Blakley, C.; Korose, C.; Okwen, R. *Computed Tomography Scanning and Geophysical Measurements of the CarbonSAFE Seal Integrity Wells in the Illinois Basin;* DOE/NETL-2023/4323; NETL Technical Report Series; U.S. Department of Energy, National Energy Technology Laboratory: Morgantown, WV, 2023; p 68. DOI: https://doi.org/10.2172/1962306

An electronic version of this report can be found at:

https://netl.doe.gov/energy-analysis/search/search

https://edx.netl.doe.gov/carbonstorage

The data in this report can be accessed from NETL's Energy Data eXchange (EDX) online system (https://edx.netl.doe.gov) using the following link: https://edx.netl.doe.gov/dataset/isgs-seal-wells

Computed Tomography Scanning and Geophysical Measurements of the CarbonSAFE Seal Integrity Wells in the Illinois Basin

Thomas Paronish[1,2], Natalie Mitchell[1,2], Sarah Brown[1,2], Mathias Pohl[1,2], Dustin Crandall[1], Curt Blakley[3], Christopher Korose[3], Roland Okwen[3]

[1]National Energy Technology Laboratory, 3610 Collins Ferry Road, Morgantown, WV 26505

[2]NETL Support Contractor, 3610 Collins Ferry Road, Morgantown, WV 26505

[3] Illinois State Geological Survey, 615 E. Peabody, Champaign, IL 61820

DOE/NETL-2023/4323

20 March 2023

NETL Contacts:

Dustin Crandall, Principal Investigator and Technical Portfolio Lead

Bryan Morreale, Associate Laboratory Director for Research & Innovation, Research & Innovation Center

This page intentionally left blank.

Table of Contents

This page intentionally left blank.

List of Figures

List of Figures (cont.)

List of Tables

This page intentionally left blank.

Acronyms, Abbreviations, and Symbols

Term	Description
2D	Two-dimensional
3D	Three-dimensional
CarbonSAFE	Carbon Storage Assurance Facility Enterprise
CT	Computed tomography
CTN	Computed tomography number
DOE	U.S. Department of Energy
EDX	NETL's Energy Data eXchange
GM	Geophysical Monitor
H	External magnetic field
HU	Hounsfield Units
IBDP	Illinois Basin-Decatur Project
IL-ICCS	Illinois Industrial Carbon Capture and Storage
ISGS	Illinois State Geological Survey
J	Magnetic response (per unit volume)
k	Volume susceptibility
MSCL	Multi-Sensor Core Logger
NETL	National Energy Technology Laboratory
ORISE	Oak Ridge Institute for Science and Education
ρ_B	Bulk Density
XRF	X-ray fluorescence
v	Acoustic Velocity
VW	Verification Well
Z	Acoustic impedance

Acknowledgments

This work was completed at the National Energy Technology Laboratory (NETL) with support from the U.S. Department of Energy's (DOE) Office of Fossil Energy and Carbon Management. The authors wish to acknowledge Bryan Morreale (NETL Research & Innovation Center), Mark McKoy (NETL Technology Development and Integration Center), and Darin Damiani (DOE Office of Fossil Energy and Carbon Management) for programmatic guidance, direction, and support.

The authors would like to thank Bryan Tennant and Scott Workman for data collection and technical support. The authors would like to thank the staff of the Geologic Characterization, Analytics and Modeling Laboratory for continued laboratory support. This research was supported in part by an appointment from the NETL Research Participation Program, sponsored by the U.S. DOE and administered by the Oak Ridge Institute for Science and Education (ORISE).

ABSTRACT

The U.S. Department of Energy's (DOE) National Energy Technology Laboratory (NETL) researchers in Morgantown, West Virginia, utilized computed tomography (CT) facilities and the Multi-Sensor Core Logger (MSCL) to evaluate the integrity of three cores (Geophysical Monitor #2 (GM2), Verification Well #1 (VW #1), and Wabash #1 for the Illinois Basin Carbon Storage Assurance Facility Enterprise (CarbonSAFE) efforts. This work was carried out in collaboration with the Illinois State Geological Survey (ISGS) as part of their efforts to analyze cores from two field locations, including the Illinois Basin-Decatur Project (IBDP) and second stage Illinois Industrial Carbon Capture and Storage (IL-ICCS) sites at Decatur, Illinois, and the Wabash CarbonSAFE project at the Wabash Valley Resources Integrated Gasification Combined Cycle plant in Terre Haut, Indiana. The results of this study are presented in several formats and are available online on the Energy Data eXchange (EDX)(https://edx.netl.doe.gov/dataset/isgs-seal-wells).

The rock characterization was conducted using non-destructive techniques, allowing for future analysis of the cores. While the equipment used did not provide direct visualization of shale pore space, it allowed for detection of fractures and discontinuities. Low resolution CT imagery with the NETL medical CT scanner was performed on the entire core. Qualitative analysis of the medical CT images, coupled with x-ray fluorescence (XRF), P-wave, and magnetic susceptibility measurements from the MSCL were utilized to identify areas of interest for further study as well as fractured zones. The ability to quickly identify key areas for more detailed study with higher resolution will save time and resources in future studies. The combination of methods used provided a multi-scale analysis of this core and provided both a macro and micro description of the core that is relevant for many subsurface energy-related examinations traditionally performed at NETL.

1. INTRODUCTION

The U.S. Department of Energy's (DOE) National Energy Technology Laboratory (NETL) is focused on diminishing existing and future carbon dioxide (CO_2) emissions. To support this goal, NETL is studying the potential for CO_2 storage in subsurface geological reservoirs and seals. To aid in this research, NETL has established a systematic approach for evaluating core materials.

This study focuses on evaluating proposed seals for CO_2 injection into the Mt. Simon sandstone as part of Illinois Basin Carbon Storage Assurance Facility Enterprise (CarbonSAFE) efforts. The aim is to gather comprehensive data through CT imaging and core petrophysical measurements, creating a digital representation of the core to preserve the core for further analyses. The results of this study are presented in several formats and are available online on the Energy Data eXchange (EDX) (https://edx.netl.doe.gov/dataset/isgs-seal-wells). This report is intended to provide the data for others to use but does not include a site characterization or in-depth analysis.

1.1 STUDY AREA

This study characterizes three wells from two Illinois Basin project locations: The Wabash #1 well (IGWS_ID: 168045) drilled in association with the Wabash CarbonSAFE project; the Verification Well #1 (VW #1) well (API: 12-115-2346000) drilled on the Illinois Basin – Decatur Project site (IBDP) in the first phase of the project; and the (Geophysical Monitor #2 (GM #2) well (API: 12-115-2359400) drilled as part of the follow-up Illinois Industrial Carbon Capture and Storage (IL-ICCS) project.

Both the VW #1 well and GM #2 wells were drilled in association with the IBDP and IL/ICCS field projects, which demonstrated the potential for commercial-scale carbon capture and storage from Archer Daniels Midland's ethanol production facility (Blakley et al., 2019). The VW #1 is part of the IBDP outside of Decatur, Illinois in Macon County (lat. 39.879795, long. -88.893359) and was drilled in association with a Class VI permit issued in 2014. The GM #2 is part of the IL-ICCS outside of Decatur, Illinois in Macon County (lat. 39.884702, long. -88.887092), north of the IBDP site, and drilled in association with a Class VI permit issued in 2015 (Bauer et al., 2019; Blakley et al., 2019).

The Wabash #1 well (IGWS_ID: 168045) is a stratigraphic test well located at the Wabash Valley Resources facility near Terre Haute, Indiana, in Vigo County (lat. -87.427426, long. 39.531626). The Wabash Valley Resources Integrated Gasification Combined Cycle plant at Terre Haute, Indiana, plans to collect carbon dioxide from the production of hydrogen at the repurposed plant (Wabash Valley Resources, 2021; Energy.gov, 2021). The Wabash #1 well was permitted on Nov. 12, 2019, and reached a total depth of 8,739 ft, finishing in the Cambrian-age sandstone on Feb. 7, 2020. In the deeper (total depth) section of the well, core was collected from the Eau Claire shale and Mt. Simon sandstone; only analysis of the Eau Claire shale section of core is presented in this report (Korose and Whittaker, 2020). Characterization of the Mt. Simon for this well can be found on EDX at (https://edx.netl.doe.gov/dataset/wabash-no-1-well) (Paronish et al., 2021), and (https://edx.netl.doe.gov/dataset/illinois-state-geological-survey-isgs-wabash-carbonsafe-well-information) (ISGS, 2022).

1.2 CORE DESCRIPTION

The GM #2 core consists of two distinct zones, between 2,600 to 2,636.9 ft, and between 2,790 to 2,825.6 ft. The first is the upper Maquoketa/Silurian contact, and second is the Galena/Maquoketa contact representing the basal contact of the Maquoketa shale. The Maquoketa is a gray to dark gray mudrock, while the Silurian and Galena limestones are light-gray to gray mudstones to wackestones, heavily bioturbated and fractured.

The VW #1 core characterized was drilled in the Eau Claire shale, between 5,425 to 5,562 ft. The core consists of interbedded layers of shale and siltstone, heavily bioturbated. The upper part of the core is predominantly composed of clay, while the lower part is dominated by quartz.

The Wabash #1 well features two core sections, one from the Maquoketa shale (between 2,435 to 2,493 ft) and one from the Eau Claire shale (between 6,104 to 6,171 ft). The Maquoketa shale core is composed of dark gray to gray mudstone with some foot-to-sub-foot intervals of wackestone and is gray to dark gray in color. The Eau Claire shale in the Wabash # 1 well is a mixture of interbedded shale and siltstone, with a heavily bioturbated structure and a slight increase in sandy intervals at the base of the well.

1.3 CORE PHOTOGRAPHS

GM #2 Well

2,600–2,605.6 ft

2,605.6–2,611.3 ft

2,611.3–2,617 ft

2,617–2,621.7 ft

Figure 1: Photographs of GM #2 well from 2,600 to 2,621.7 ft.

2,621.7–2,627.3 ft

2,627.3–2,633 ft

2,633–2,636.9 ft

Figure 2: Photographs of GM #2 well from 2,621.7 to 2,636.9 ft.

2,790–2,796 ft

2,796–2,801.6 ft

2,801.6–2,807 ft

2,807–2,812 ft

Figure 3: Photographs of GM #2 well from 2,790 to 2,812 ft.

2,812–2,817.7 ft **2,817.7–2,823 ft**

2,823–2,825.6 ft

Figure 4: Photographs of GM #2 well from 2,812 to 2,825.6 ft.

VW #1 Well

5,425–5,431 ft **5,431–5,436 ft**

5,436–5,441.7 ft **5,441.7–5,447.5 ft**

Figure 5: Photographs of VW #1 well from 5,425 to 5,447.5 ft.

5,447.5–5,453 ft

5,453–5,485.5 ft

5,458.5–5,464 ft

5,464–5,469 ft

Figure 6: Photographs of VW #1 well from 5,447.5 to 5,469 ft.

5,469–5,474.5 ft

5,474.5–5,480 ft

5,480–5,485.5 ft

5,485.5–5,491 ft

Figure 7: Photographs of VW #1 well from 5,469 to 5,491 ft.

5,491–5,497 ft **5,497–5,502.5 ft**

5,502.5–5,508.3 ft **5,508.3–5,515 ft**

Figure 8: Photographs of VW #1 well from 5,491 to 5,515 ft.

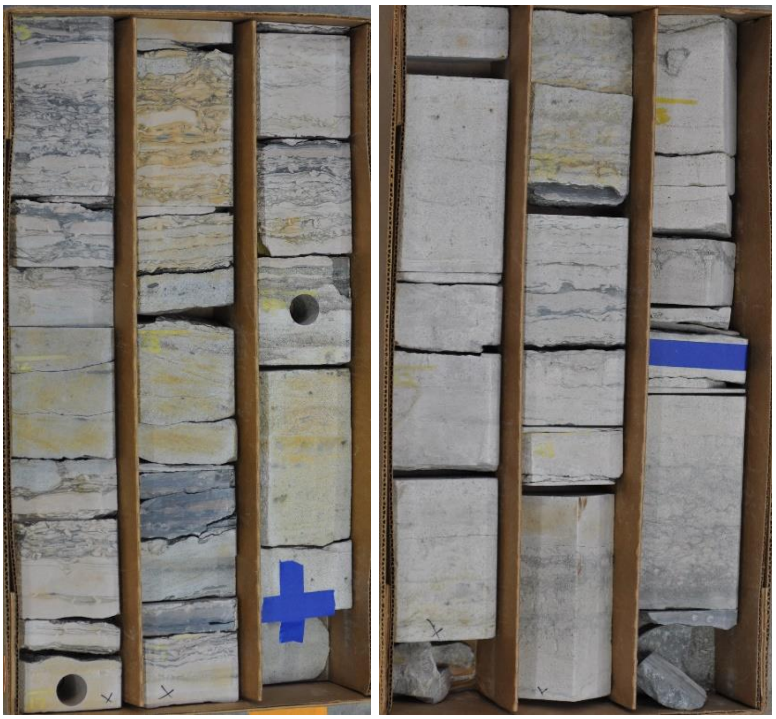

5,515–5,520.8 ft **5,520.8–5,527 ft**

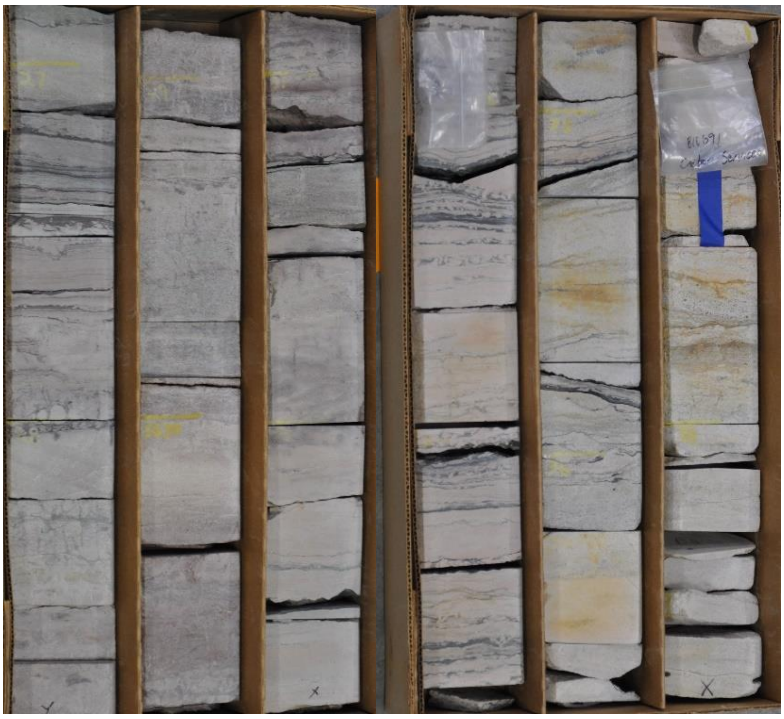

5,527–5,533 ft **5,533–5,538.7 ft**

Figure 9: Photographs of VW #1 well from 5,515 to 5,538.7 ft.

5,538.7–5,544.5 ft

5,544.5–5,550.4 ft

5,550.4–5,556.2 ft

5,556.2–5,562 ft

Figure 10: Photographs of VW #1 well from 5, 538.7 to 5,562 ft.

Wabash #1

2,435–2,440.7 ft

2,440.7–2,446.6 ft

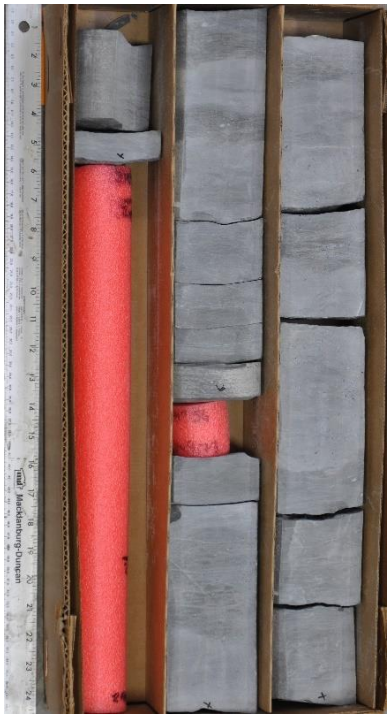

2,446.6–2,453.3 ft

2,453.3–2,458.12 ft

Figure 11: Photographs of Wabash #1 well from 2,435 to 4,458.12 ft

2,458.12–2,463.93 ft

2,463.93–2,469.84 ft

2,469.84–2,475.7 ft

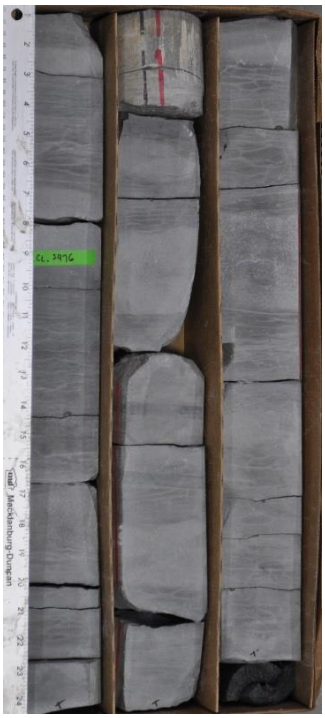

2,475.7–2,481.35 ft

Figure 12: Photographs of Wabash #1 well from 2,458.12 to 2,481.35 ft.

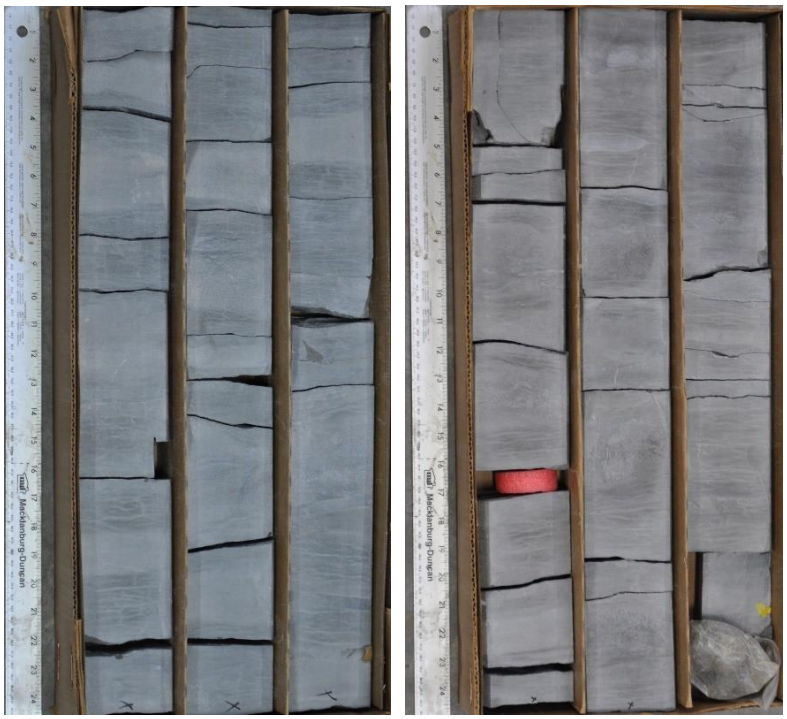

2,481.35–2,487.2 ft **2,487.2–2,493.05 ft**

Figure 13: Photographs of Wabash #1 well from 2,481.35 to 2,493.05 ft.

6,104–6,110.07 ft **6,110.07–6,115.85 ft**

6,115.85–6,121.5 ft **6,121.5–6,127.42 ft**

Figure 14: Photographs of Wabash #1 well from 6,104 to 6,127.42 ft.

6,133.19–6,139.14 ft

6,139.14–6,145 ft

6,145–6,150.6 ft

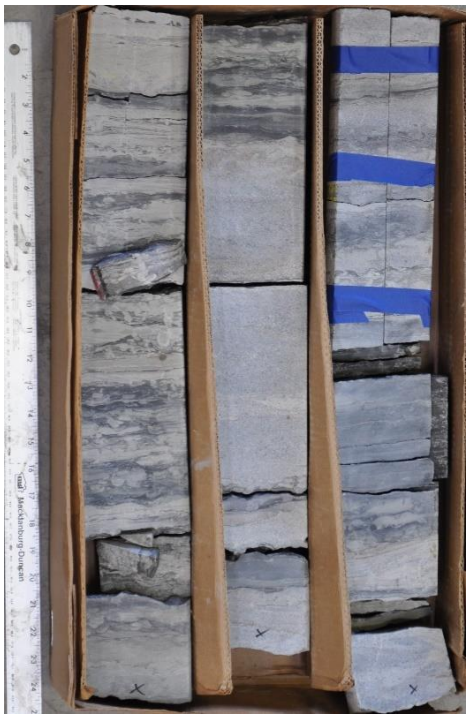

6,150.6–6,156.4 ft

Figure 15: Photographs of Wabash #1 well from 6,133.19 to 6,156.4 ft.

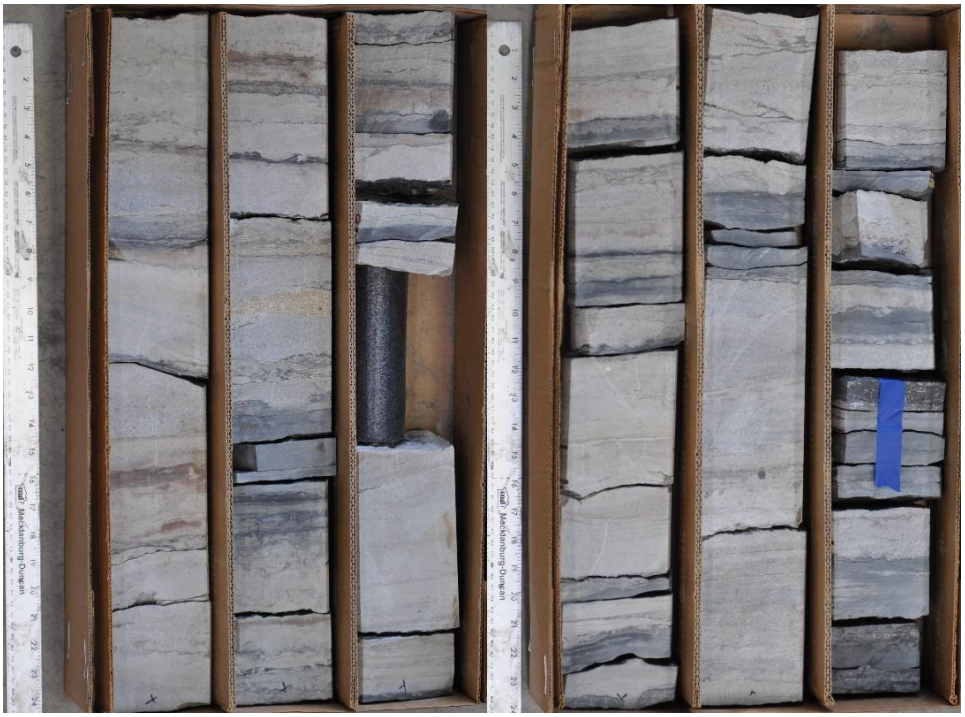

6,154.4–6,162.8 ft **6,162.8–6,168.6 ft**

6,168.6–6,171.4 ft

Figure 16: Photographs of Wabash #1 well from 6,154.4 to 6,171.4 ft.

2. DATA ACQUISITION AND METHODOLOGY

The 2/3rd slabbed core was evaluated using computed tomography (CT) scanning and traditional core logging.

2.1 CORE LOGGING

A Geotek® Multi-Sensor Core Logging (MSCL, Figure 17) system was used to conduct geophysical measurements, including core thickness deviation, P-wave travel time, magnetic susceptibility, and gamma count. For the 2/3rd slabbed core that was scanned as part of this analysis, the P-wave velocity was measured and reported. The system also measured bulk elemental chemistry with a built-in, portable X-ray fluorescence (XRF) spectrometer. For more information on the capabilities of the Geotek® MSCL system, refer to Crandall et al. (2017).

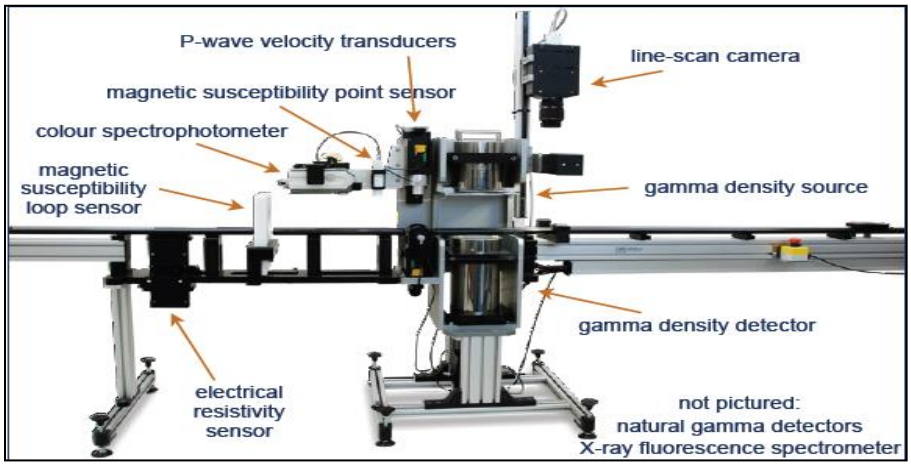

Figure 17: Representation of generalized MSCL with all attached instruments. From Geotek Ltd. (2009).

2.1.1 Magnetic Susceptibility

Magnetic susceptibility is a measure of the degree of magnetization in a sample. The sample is exposed to an external magnetic field, and magnetic susceptibility is the measured magnetic response to that field:

$$J = kH$$

Where J is the magnetic response (per unit volume), k is volume susceptibility, and H is an external magnetic field. The measurement unit is dimensionless (abbreviated simply as SI). All materials have magnetic susceptibility. Positive values of magnetic susceptibility indicate that materials are paramagnetic and occur in rocks that are majority ferromagnetic, ferrimagnetic, or antimagnetic (iron bearing) materials. Whereas negative values of magnetic susceptibility indicate that materials are diamagnetic and occur in rocks dominated by non-iron material (i.e., calcite or quartz). Table 1 lists examples of common magnetic susceptibility ranges (Hunts et al., 1995).

Magnetic susceptibility was measured using the Bartington point sensor, where a 1-cm-diameter, low-intensity (8.0 A/m RMS) non-sensitive, alternating magnetic field (2 kHz) was generated for 10 s. To minimize any potential drift in the oscillating field, the point sensor was zeroed at the beginning and end of the sample, as well as after every 5th measurement. The point sensor, due to the small field, was limited in whole core measurements and is temperature dependent (Geotek Ltd. Multi-Sensor Core Logger Manual, Version 05-10, 2010).

Table 1: Magnetic Susceptibility Values for Common Minerals (Hunts et al., 1995)

Mineral	x (*10^{-6}) SI
Water	9
Calcite	-7.5 to -39
Halite, Gypsum	-10 to -60
Shale	63 to 18,600
Illite, Montmorillonite	330 to 410
Pyrite	5 to 3,500
Chalcopyrite	23 to 400
Hematite	500 to 40,000
Magnetite	1,000,000 to 5,700,000

2.1.2 P-wave Velocity

P-wave velocity measurements were performed to measure the acoustic impedance of a geologic sample with compressional waves. Acoustic impedance is a measure of how well a material transmits vibrations, which is directly proportional to density and/or material consolidation. An example of a material that has a high acoustic impedance would be air, with a wave speed of 330 m/s, whereas granite would have low acoustic impedance, with a wave speed of >5,000 m/s. These measurements can be proxies for seismic reflection coefficients and can be translated to field use when doing seismic surveys.

The software associated with the MSCL measures the travel time of the pulse with a resolution of 50 ns. The absolute accuracy of the instrument measurements is $\pm$ 3 m/s with a resolution of 1.5 m/s (Geotek Ltd., 2010).

2.1.3 XRF Spectrometry

In addition to the geophysical measurements, a portable handheld Innov-X® XRF Spectrometer was used to measure relative elemental abundances of aggregated “light elements” up to and including sodium, and also various heavy elements, which were measured individually (Figure 18). Elemental abundances are reported relative to the total elemental composition, i.e., out of 100% weight.

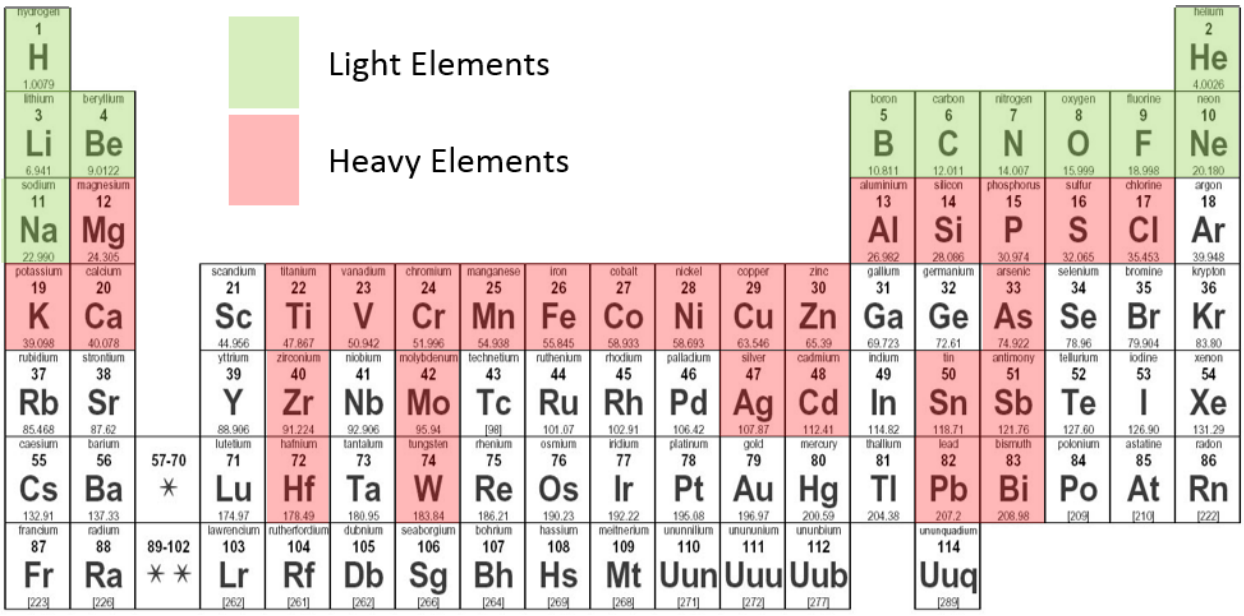

Figure 18: Periodic table showing elements measurable by the Innov-X® X-Ray Fluorescence Spectrometer (shaded).

The XRF spectrometer measures elemental abundances by subjecting the sample to X-ray photons. The high energy of the photons displaces inner orbital electrons in the respective elements. The vacancies in the lower orbitals cause outer orbital electrons to "fall" into lower orbits to satisfy the disturbed electron configuration. The substitution into lower orbitals causes a release of a secondary X-ray photon, which has an energy associated with a specific element. These relative and element-specific energy emissions can then be used to determine bulk elemental composition.

2.2 MEDICAL CT SCANNING

Core scale CT scanning was performed with a medical Toshiba® Aquilion TSX-101A/R medical scanner, as shown in Figure 19. The medical CT scanner generates images with a resolution in the millimeter range, with scans having voxel resolutions of 0.43 x 0.43 mm in the XY plane and 0.50 mm along the core axis. The scans were conducted at a voltage of 135 kV and at 200 mA. Subsequent processing and combining of stacks was performed to create three-dimensional (3D) volumetric representations of the cores and a two-dimensional (2D) cross-section through the middle of the core samples using ImageJ (Rasband, 2019). The variation in grayscale values observed in the images indicates changes in the CT number obtained from the scans, which is directly proportional to changes in the attenuation and density of the scanned rock, i.e., darker regions are less dense. Filled fractures, open fractures, and changes in bedding structure can be resolved via careful examination of the CT images. While the medical CT scanner was not used for detailed characterization in this study, it allowed for non-destructive bulk characterization of the core and thus complemented the MSCL data on the resultant logs.

Figure 19: Toshiba® Aquilion™ Multislice Helical CT Scanner at NETL used for core analysis.

2.3 MICRO-CT SCANNING

Micro-CT scanning was performed using a ZEISS Xradia MicroXCT-400 scanner. The Xradia system has the highest resolution of the scanners at NETL and scans samples sized from sub-mm to 25 mm. The Xradia provides detailed image data that can be used to infer porosity, mineralogy, and structure.

2.4 DATA COMPILATION

Strater® by Golden Software® was used to compile the MSCL and medical CT data into a series of geophysical logs. The data used to generate these logs can be accessed from NETL's EDX online system using the following link: https://edx.netl.doe.gov/dataset/isgs-seal-wells.

3. RESULTS

This section contains processed 2D slices of the medical CT scans through the cores, followed by the XRF, and magnetic susceptibility measurements of the core from the MSCL.

3.1 MEDICAL CT SCANS

The core from the GM #2, VW #1, and Wabash #1 wells was scanned with a Toshiba Aquilion TSX-101A/R medical CT scanner at a sub-mm core-scale resolution (430 µm by 430 µm by 500 µm).

As discussed previously, the variation in the grayscale values in the medical CT images indicates changes in the CT numbers (CTN), which reflects changes in the density and attenuation of the scanned rock (darker regions are less dense). Core was scanned in sections of 3 ft or less taken from each core box. In the following images, the overall depth for each scanned sub-section of core is listed and highlights interesting features such as pyrite nodules, distinct fracture planes, and fine-scale layering.

3.1.1 XZ Planes

In Figure 21 to Figure 39, a 2D image through the center of each retrieved core was generated. These are referred to as "XZ" planes and their coordinates are indicated in Figure 20. The red scale bar in the images is 2 cm and the diameter of the extracted core is 4 in. (10.16 cm) for reference. The labels under each 2D XZ plane in Figure 21 to Figure 39 show the depth at the bottom of each core and the full range of core lengths displayed in each figure is listed in the figure captions. The grayscale values have been adjusted in each of these images to best display the structure of the core.

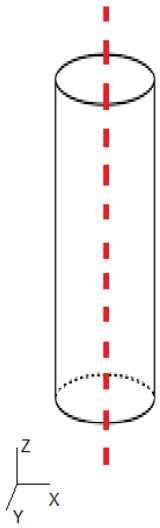

Figure 20: Schematic of the XZ isolated plane through the vertical center of the medical CT scans.

3.1.2 GM #2

2,600–2,605 ft | 2,605–2,606 ft | 2,606–2,610 ft | 2,610–2,611 ft | 2,611–2,616 ft

Figure 21: 2D isolated planes through the vertical center of the medical CT scans of the GM #2 well from 2,600 to 2,616 ft.

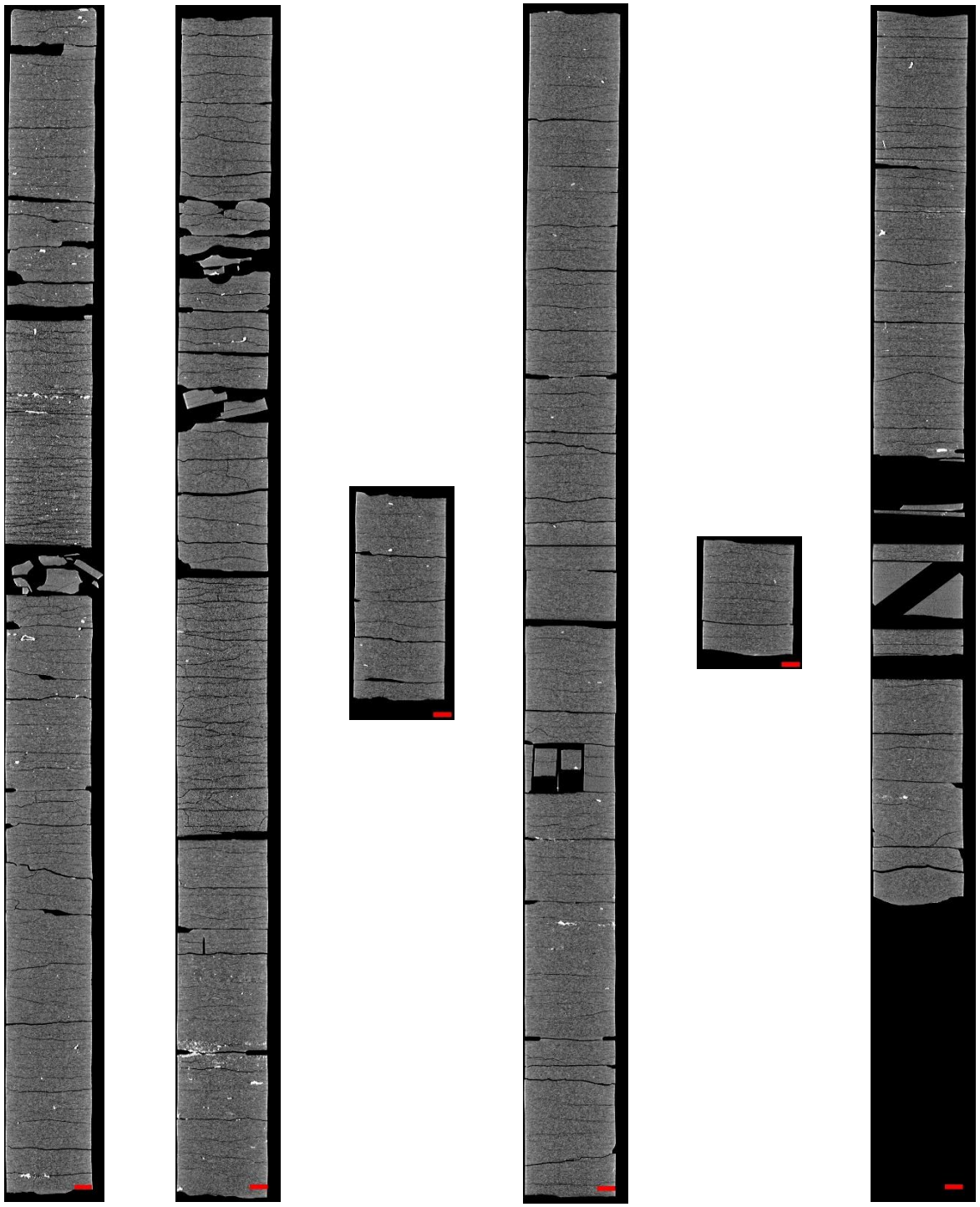

Figure 22: 2D isolated planes through the vertical center of the medical CT scans of the GM #2 well from 2,617 to 2,637 ft.

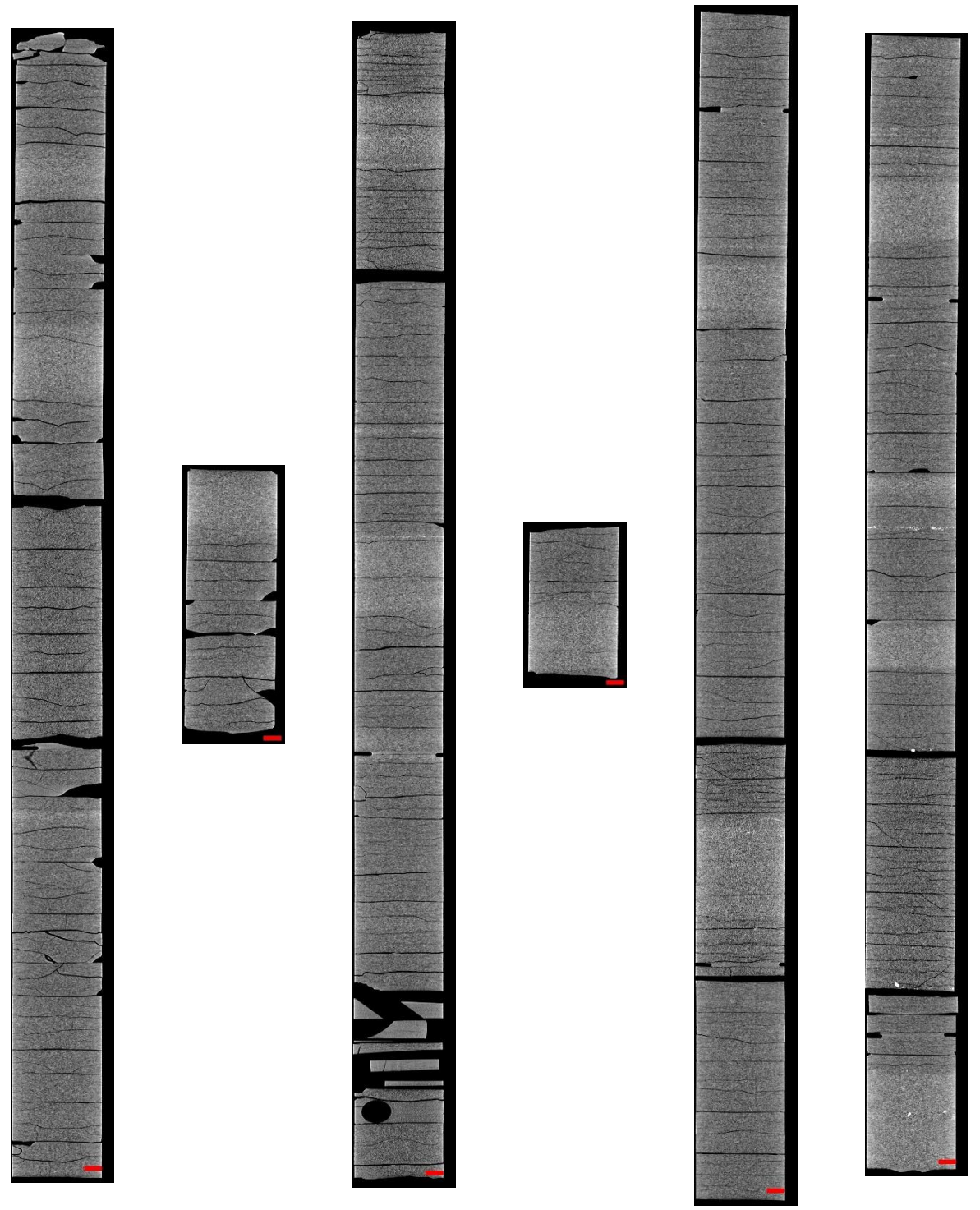

2,790–2,795 ft **2,795–2,796 ft** **2,796–2,801 ft** **2,801–2,802 ft** **2,802–2,807 ft** **2,807–2,811 ft**

Figure 23: 2D isolated planes through the vertical center of the medical CT scans of the GM #2 well from 2,790 to 2,811 ft.

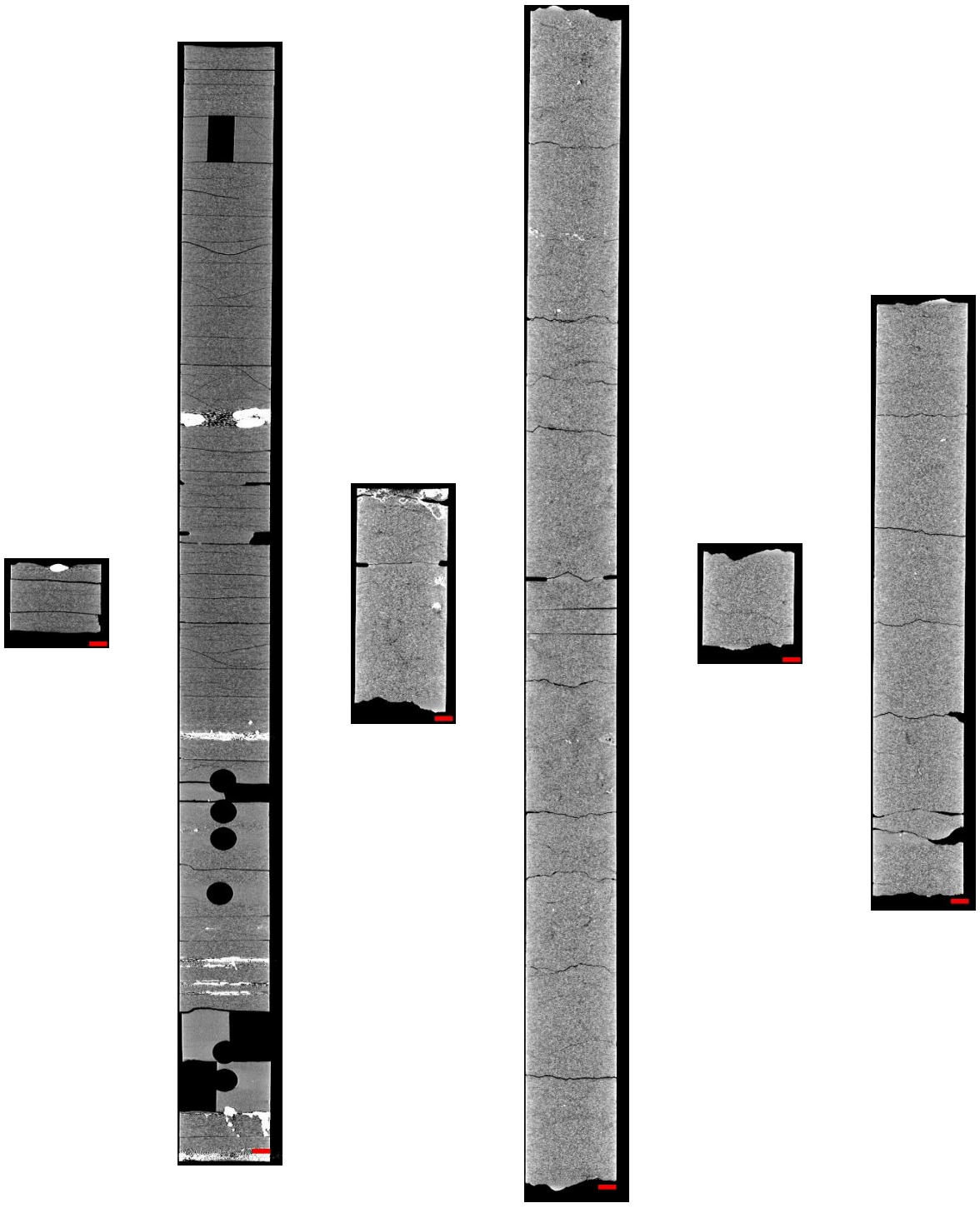

2,811–2,812 ft **2,812–2,817 ft** **2,817–2,818 ft** **2,818–2,822 ft** **2,822–2,823 ft** **2,823–2,826 ft**

Figure 24: 2D isolated planes through the vertical center of the medical CT scans of the GM #2 well from 2,811 to 2,826 ft.

3.1.3 VW #1

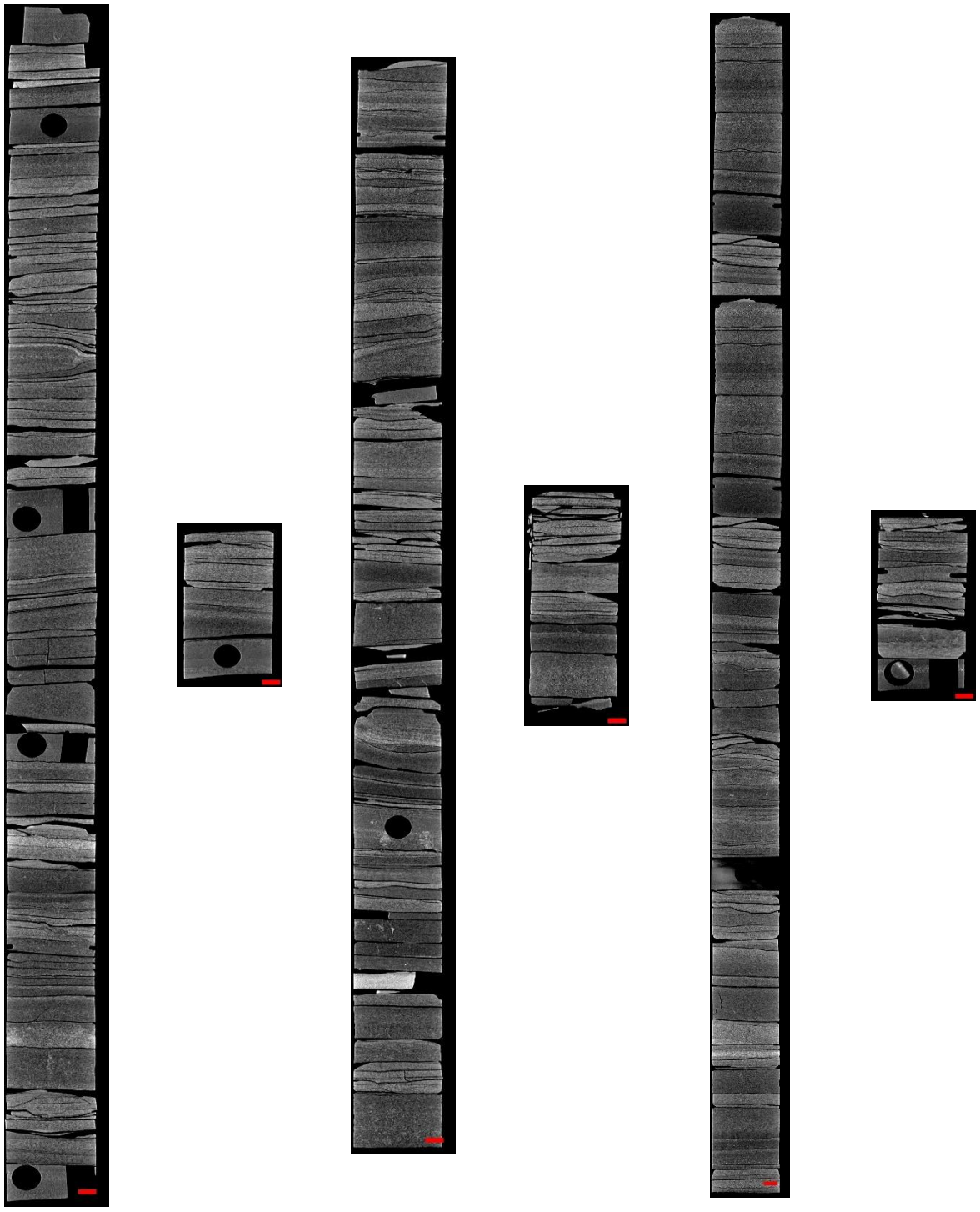

5,425–5,430 ft 5,430–5,431 ft 5,431–5,435 ft 5,435–5,436 ft 5,436–5,441 ft 5,441–5,442 ft

Figure 25: 2D isolated planes through the vertical center of the medical CT scans of the VW #1 well from 5,425 to 5,442 ft.

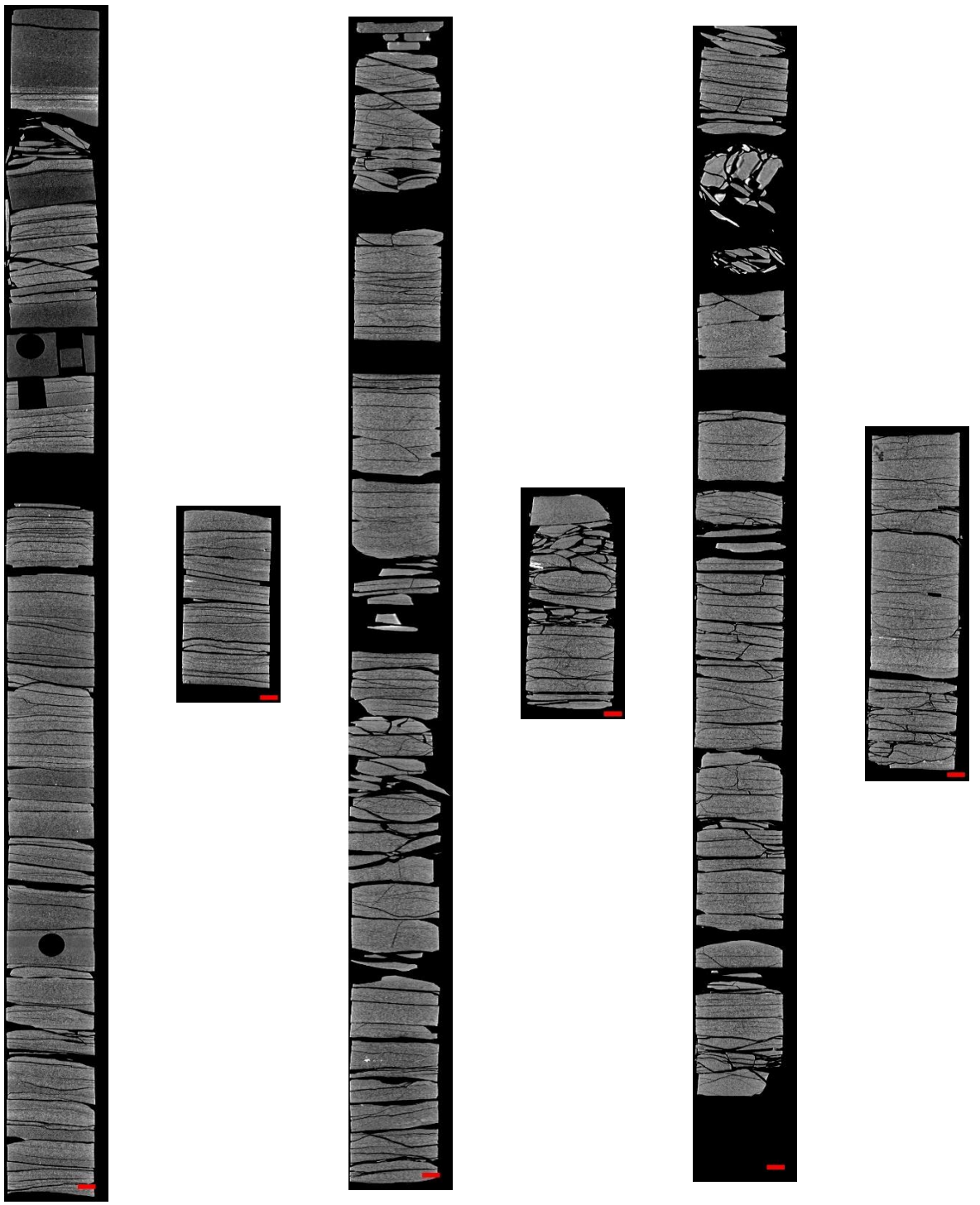

Figure 26: 2D isolated planes through the vertical center of the medical CT scans of the VW #1 well from 5,442 to 5,458 ft.

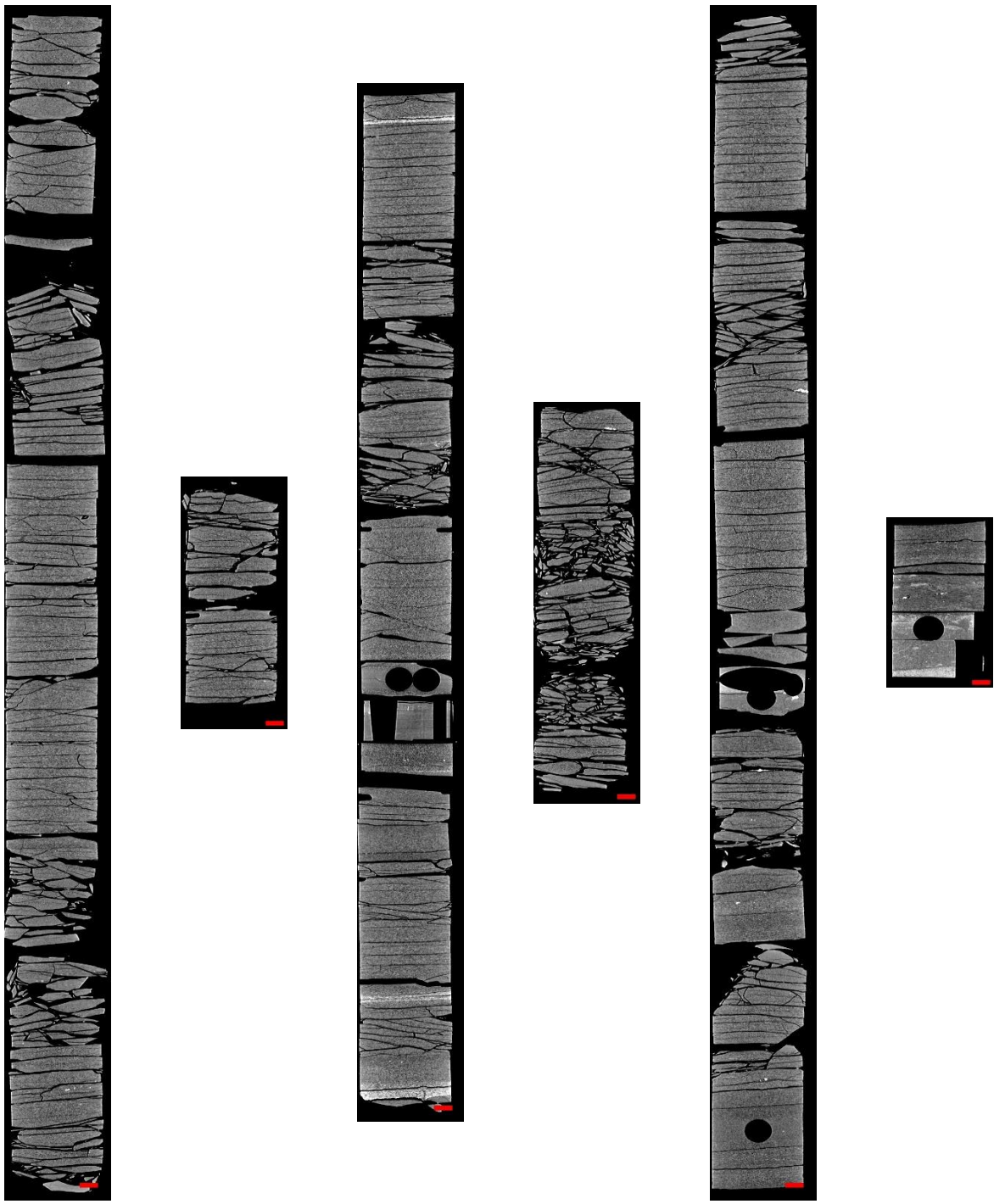

5,458–5,463 ft **5,463–5,464 ft** **5,464–5,468 ft** **5,468–5,469 ft** **5,469–5,474 ft** **5,474–5,475 ft**

Figure 27: 2D isolated planes through the vertical center of the medical CT scans of the VW #1 well from 5,458 to 5,475 ft.

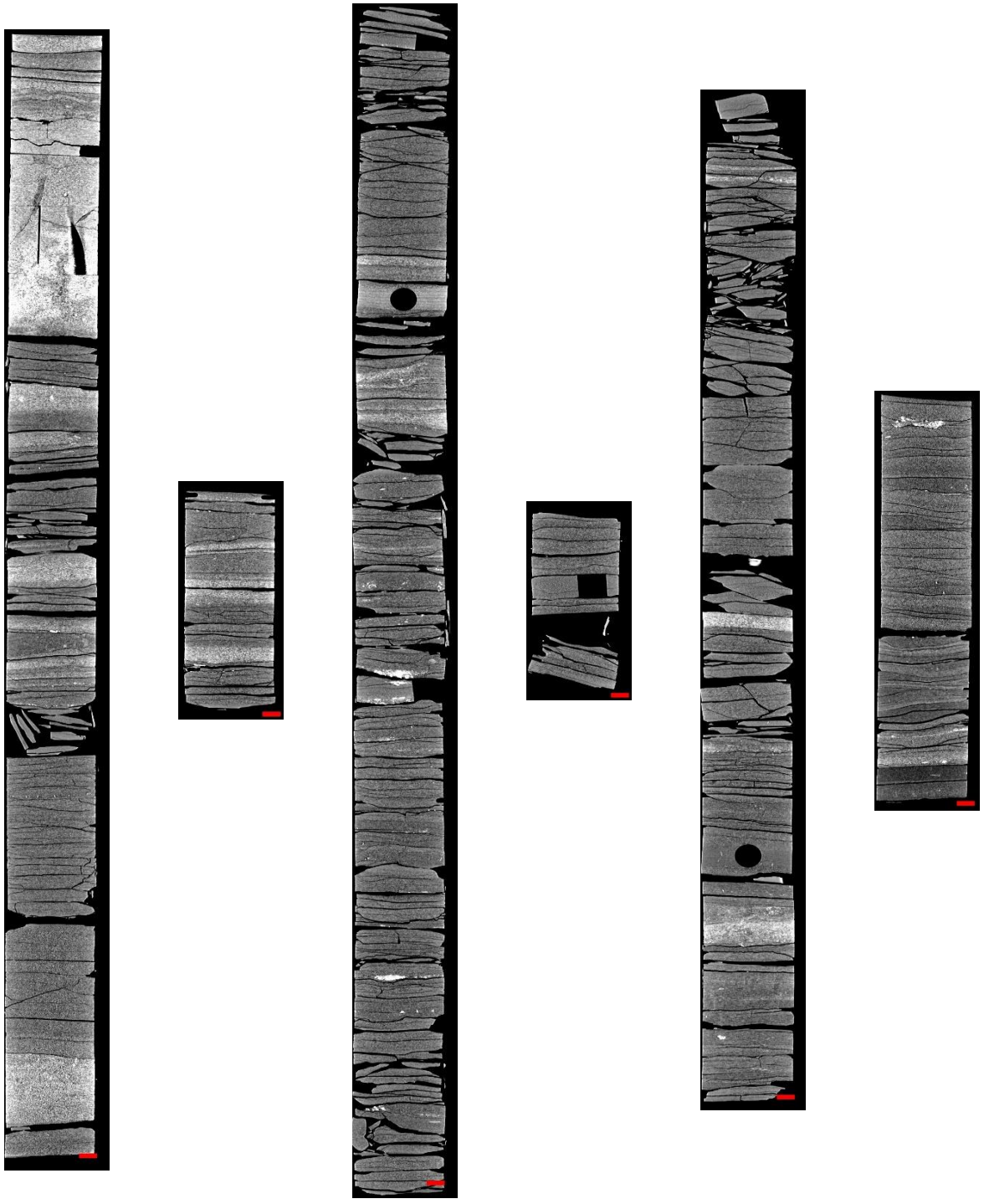

Figure 28: 2D isolated planes through the vertical center of the medical CT scans of the VW #1 well from 5,475 to 5,491 ft.

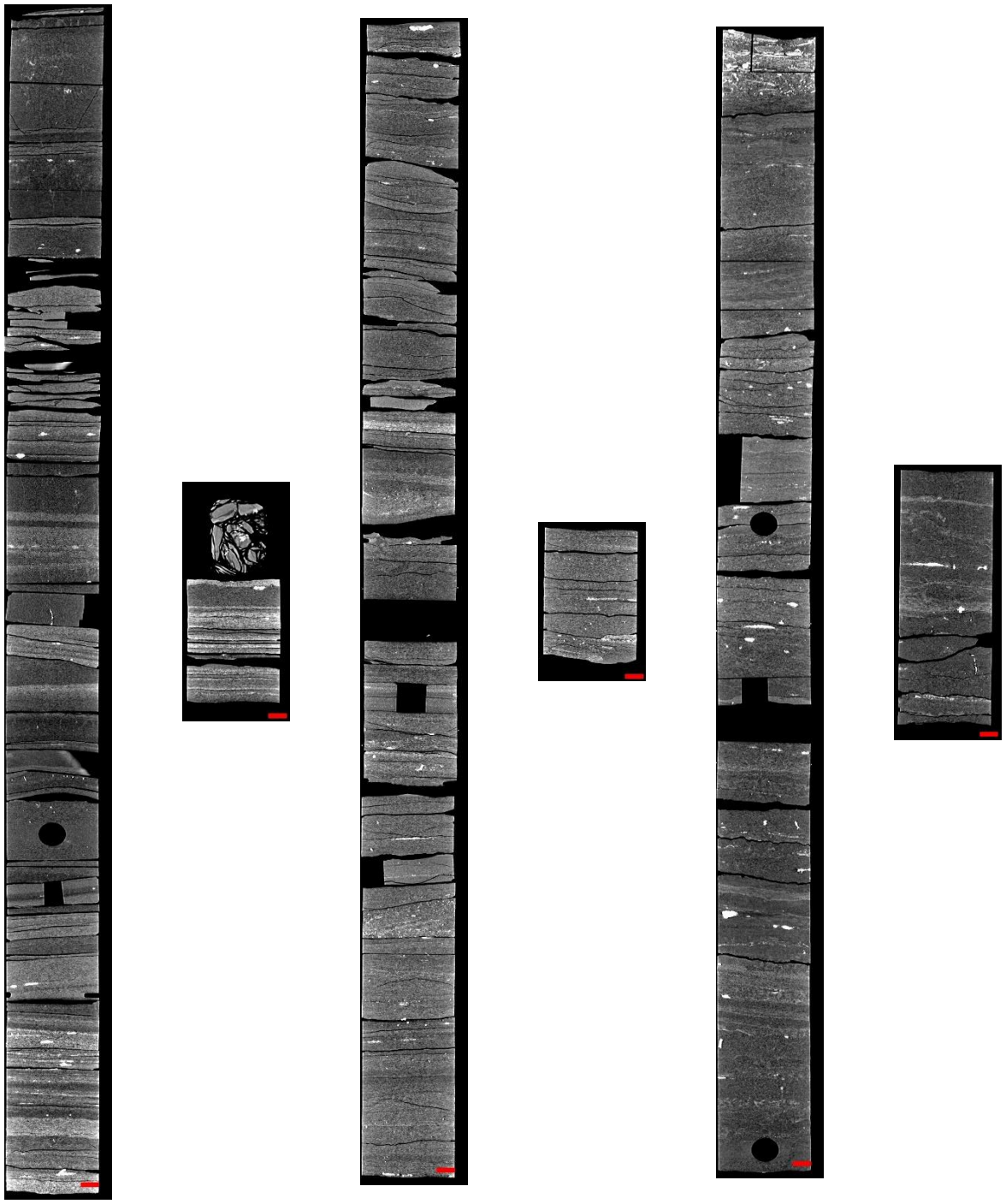

5,491–5,496 ft **5,496–5,497 ft** **5,497–5,502 ft** **5,502–5,503 ft** **5,503–5,507 ft** **5,507–5,508 ft**

Figure 29: 2D isolated planes through the vertical center of the medical CT scans of the VW #1 well from 5,491 to 5,508 ft.

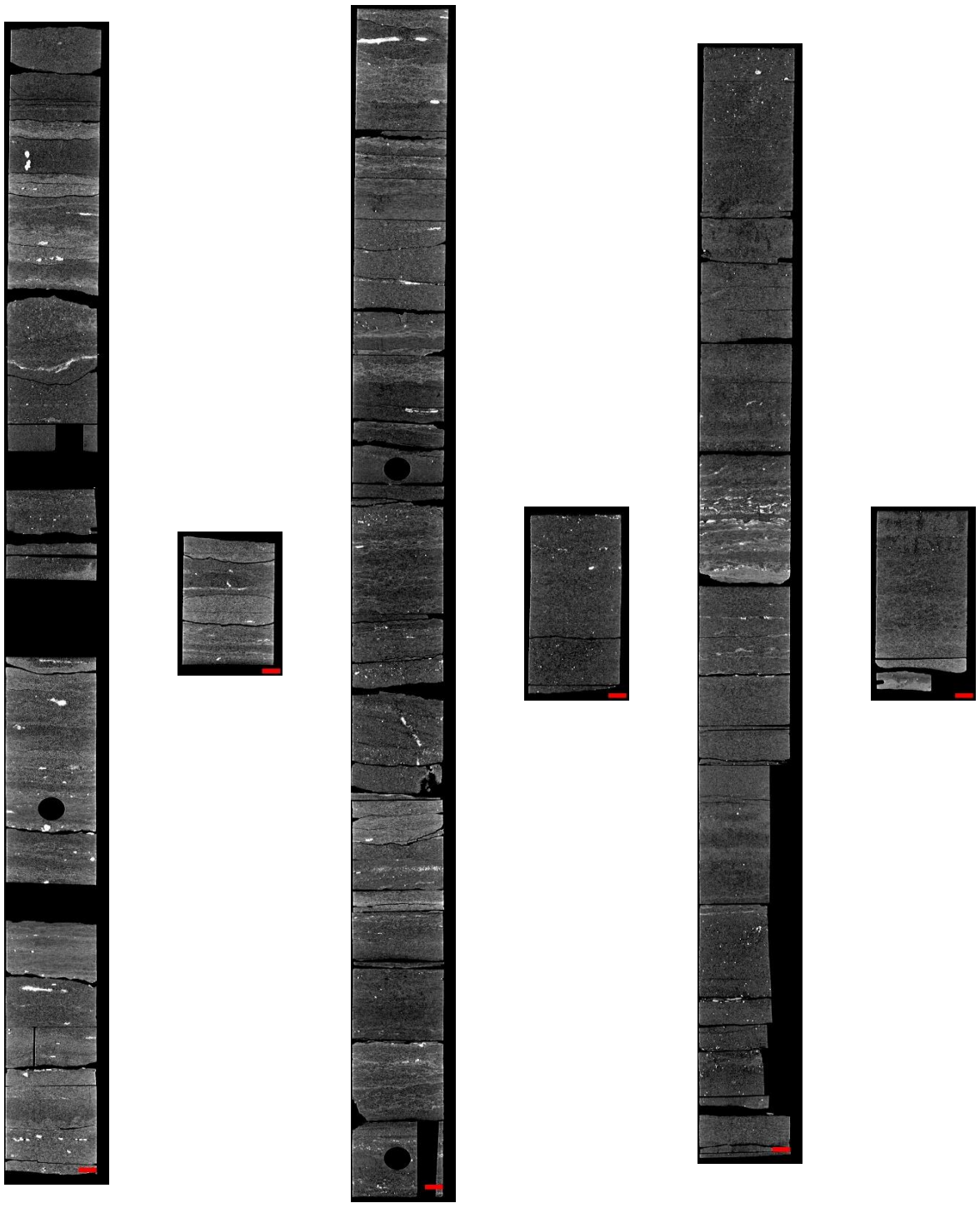

Figure 30: 2D isolated planes through the vertical center of the medical CT scans of the VW #1 well from 5,508 to 5,527 ft.

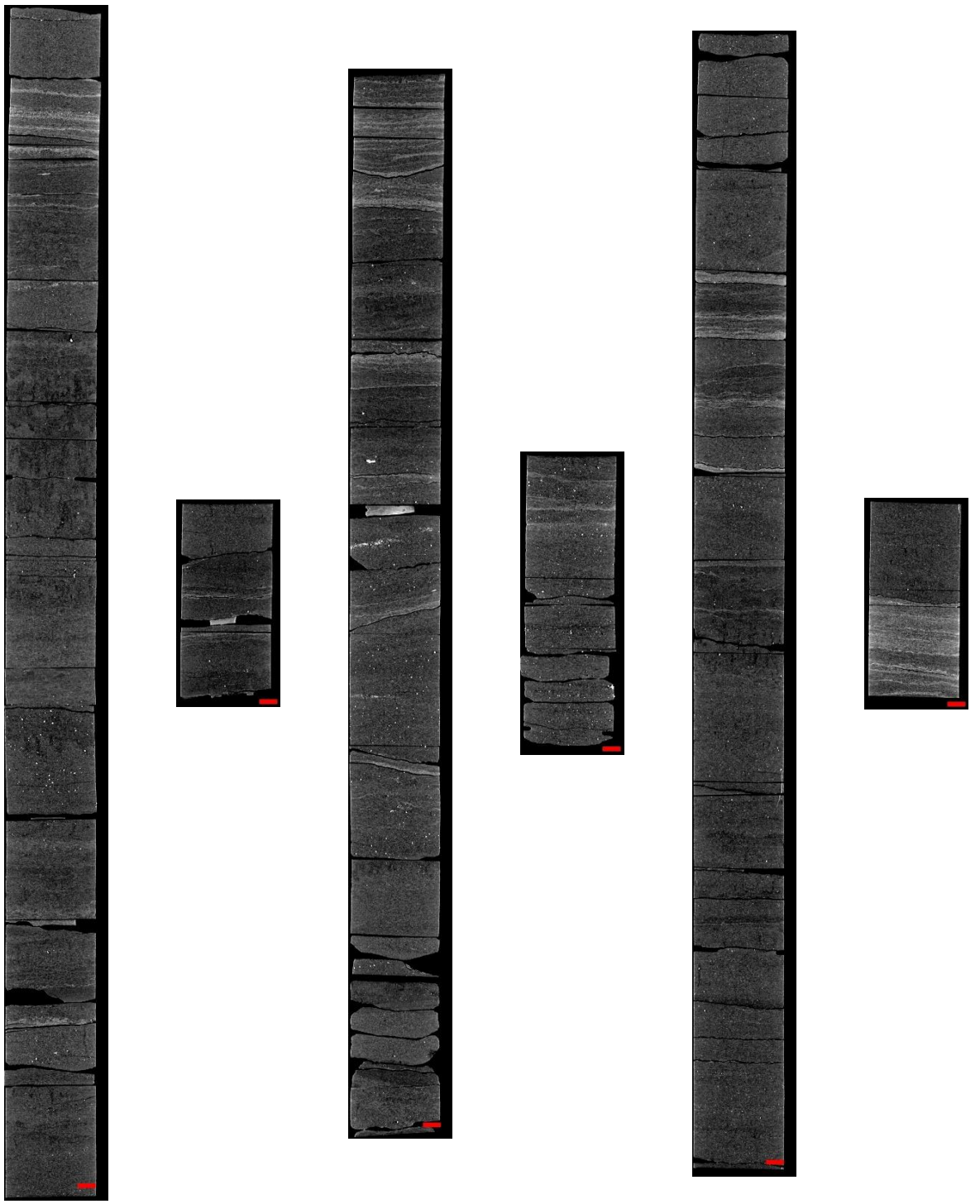

Figure 31: 2D isolated planes through the vertical center of the medical CT scans of the VW #1 well from 5,527 to 5,545 ft.

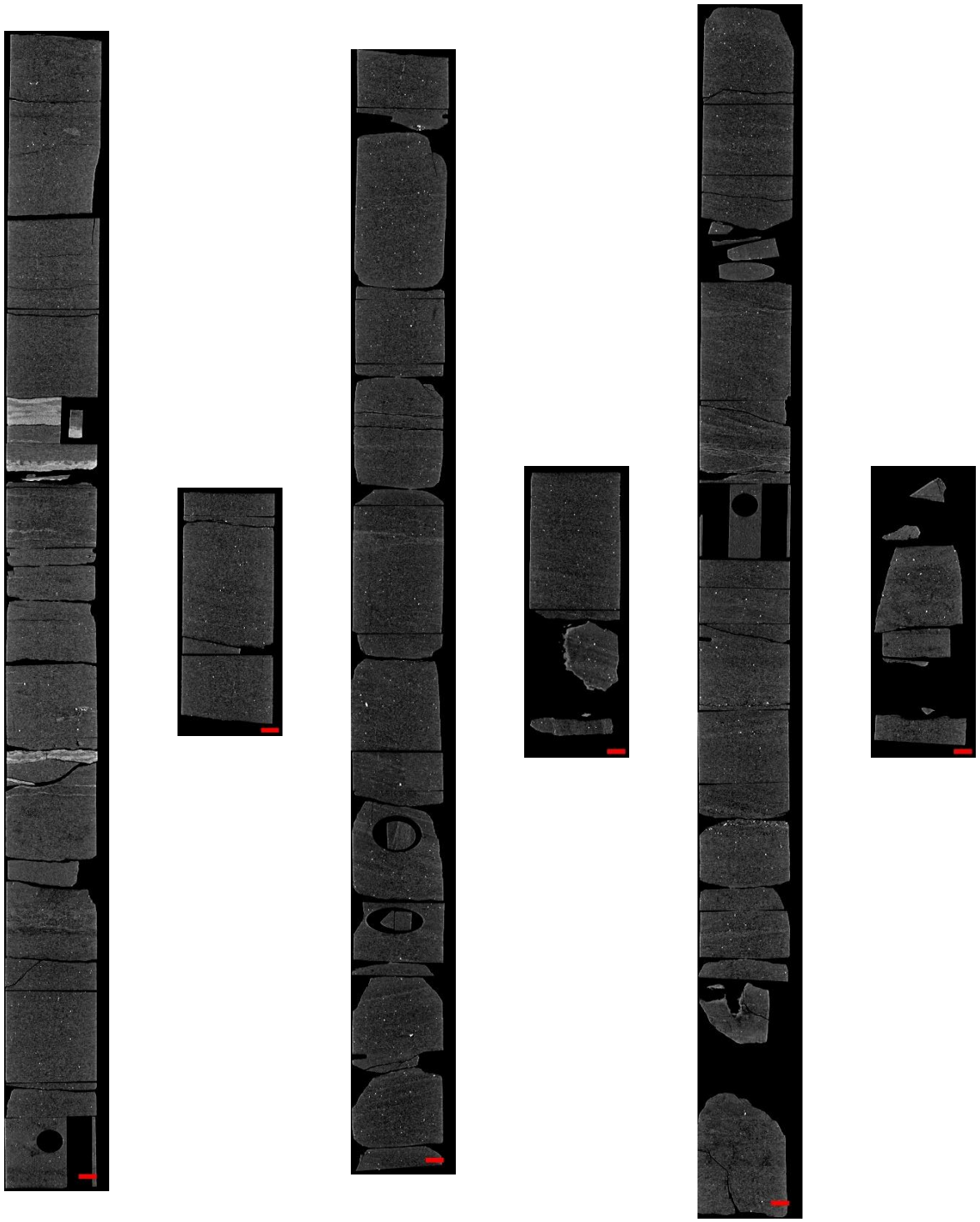

5,545–5,549 ft **5,549–5,550 ft** **5,550–5,555 ft** **5,555–5,556 ft** **5,556–5,561 ft** **5,561–5,562 ft**

Figure 32: 2D isolated planes through the vertical center of the medical CT scans of the VW #1 well from 5,545 to 5,562 ft.

3.1.4 Wabash #1

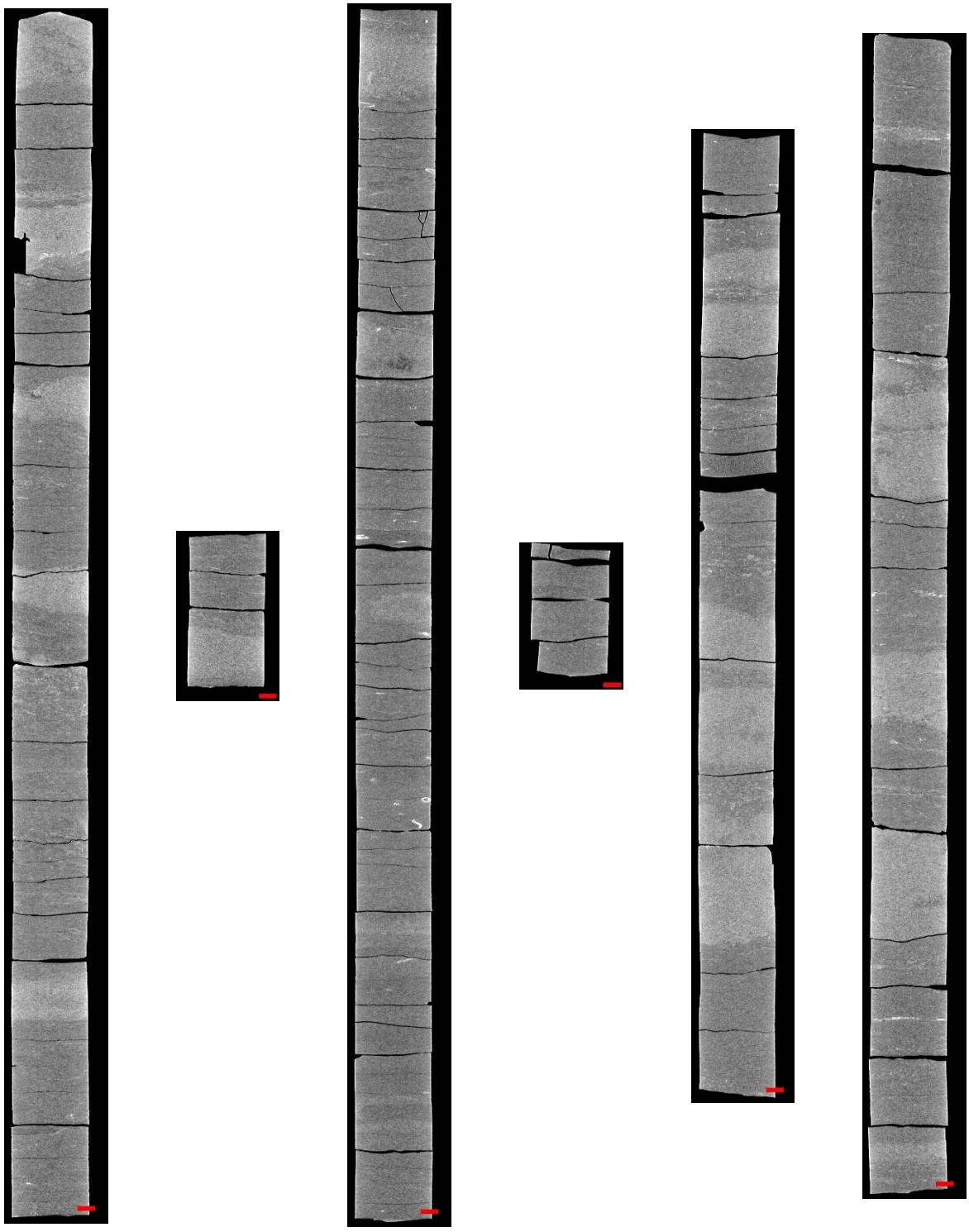

2,435–2,440 ft **2,440–2,441 ft** **2,441–5,445 ft** **2,445–2,446 ft** **2,446–2,452 ft** **2,452–2,457 ft**

Figure 33: 2D isolated planes through the vertical center of the medical CT scans of the Wabash #1 well from 2,435 to 2,457 ft.

Figure 34: 2D isolated planes through the vertical center of the medical CT scans of the Wabash #1 well from 2,457 to 2,476 ft.

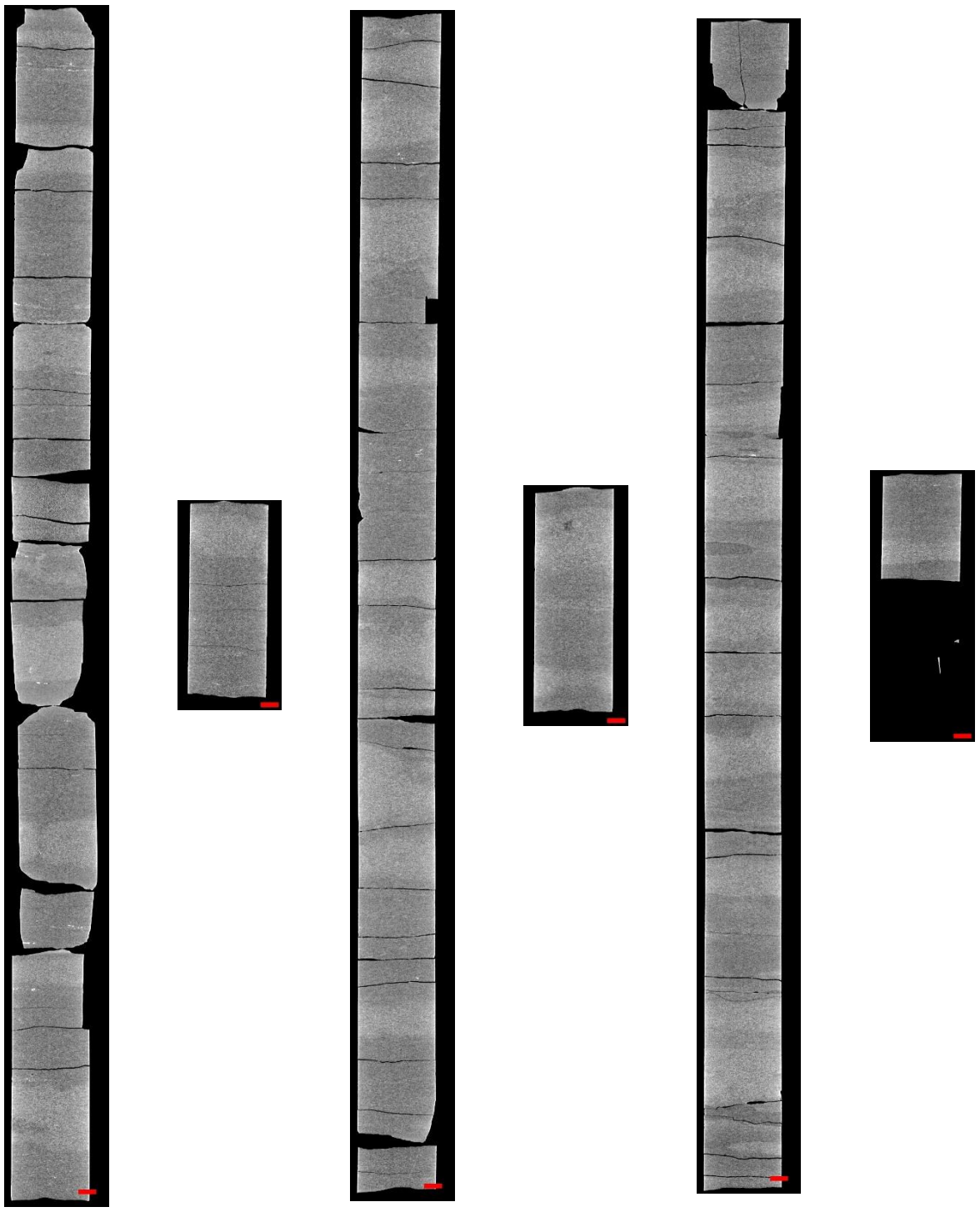

2,476–2,480 ft **2,480–2,481 ft** **2,481–2,486 ft** **2,486–2,487 ft** **2,487–2,492 ft** **2,492–2,493 ft**

Figure 35: 2D isolated planes through the vertical center of the medical CT scans of the Wabash #1 well from 2,476 to 2,493 ft.

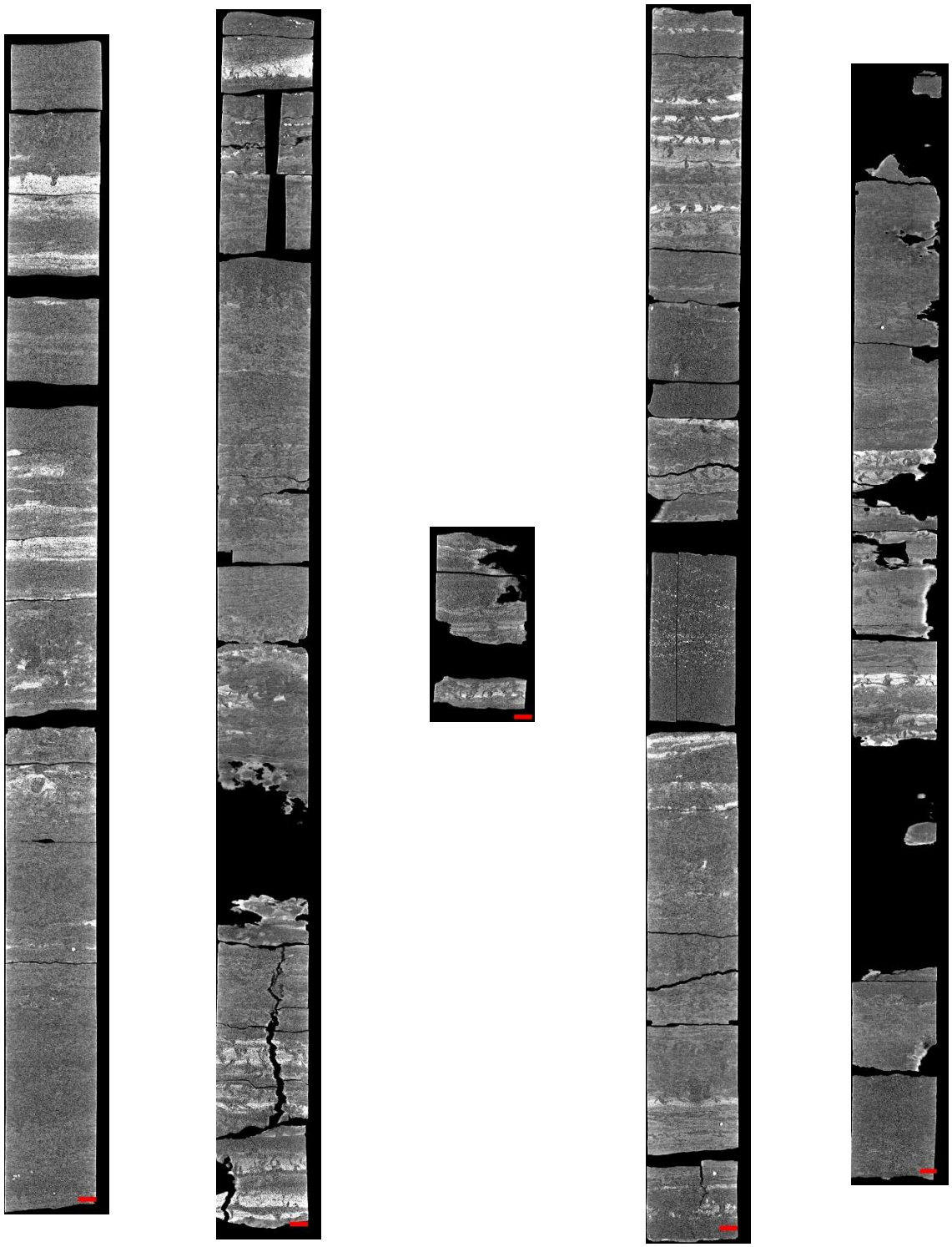

6,104–6,110 ft **6,110–6,115 ft** **6,115–6,116 ft** **6,116–6,120 ft** **6,120–6,121 ft**

Figure 36: 2D isolated planes through the vertical center of the medical CT scans of the Wabash #1 well from 6,104 to 6,121 ft.

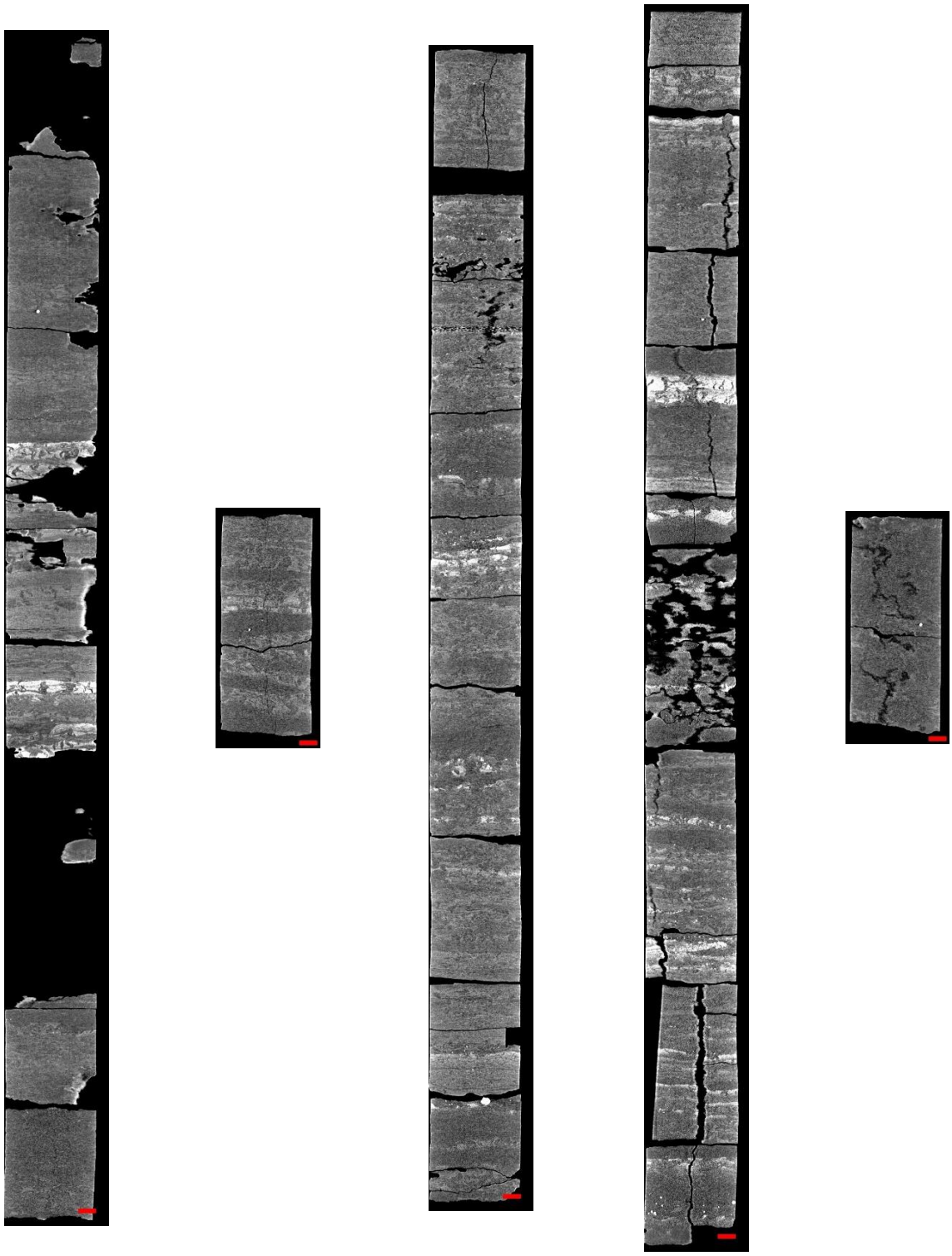

6,121–6,126 ft **6,126–6,127 ft** **6,127–6,133 ft** **6,133–6,138 ft** **6,138–6,139 ft**

Figure 37: 2D isolated planes through the vertical center of the medical CT scans of the Wabash #1 well from 6,121 to 6,139 ft.

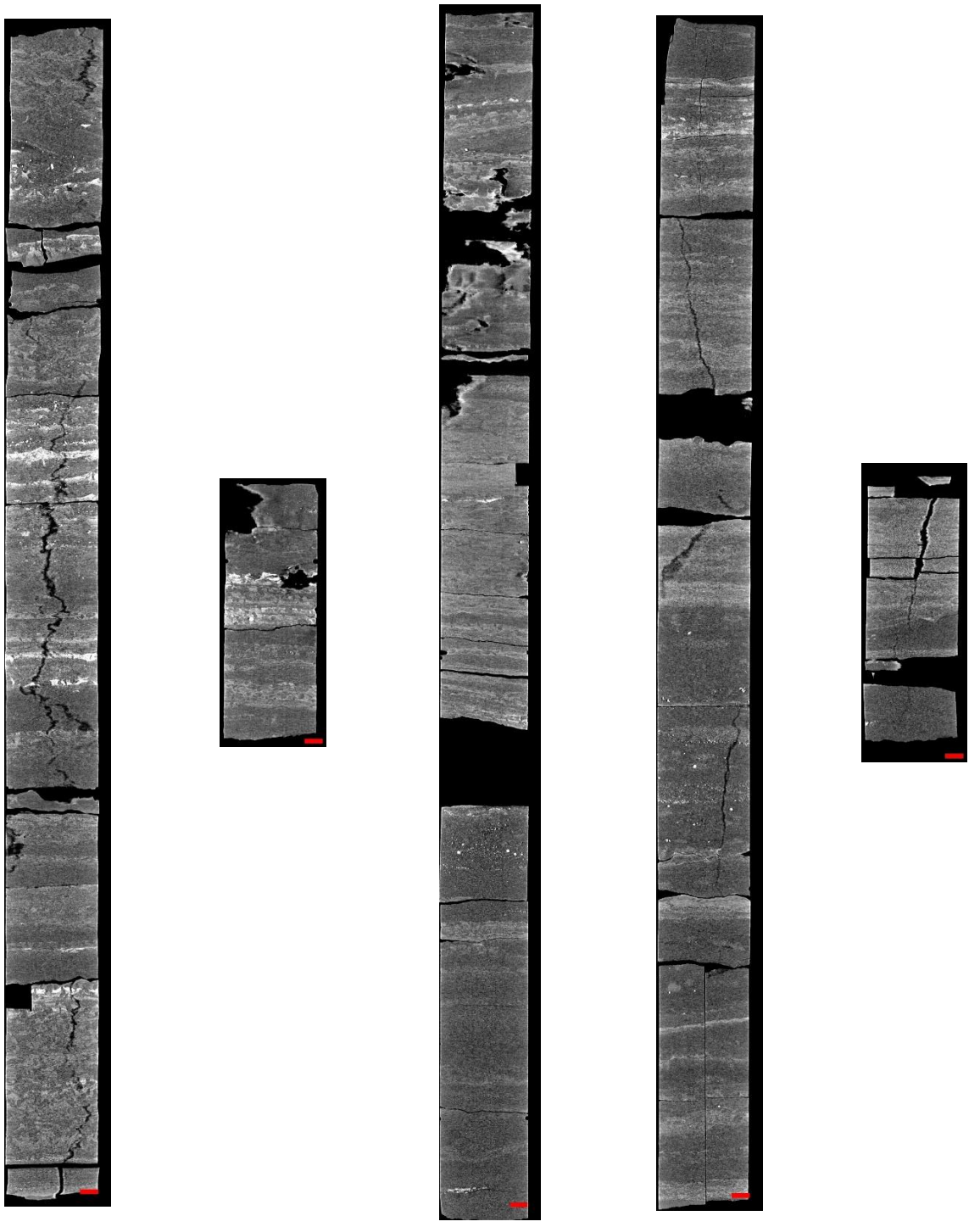

Figure 38: 2D isolated planes through the vertical center of the medical CT scans of the Wabash #1 well from 6,139 to 6,156 ft.

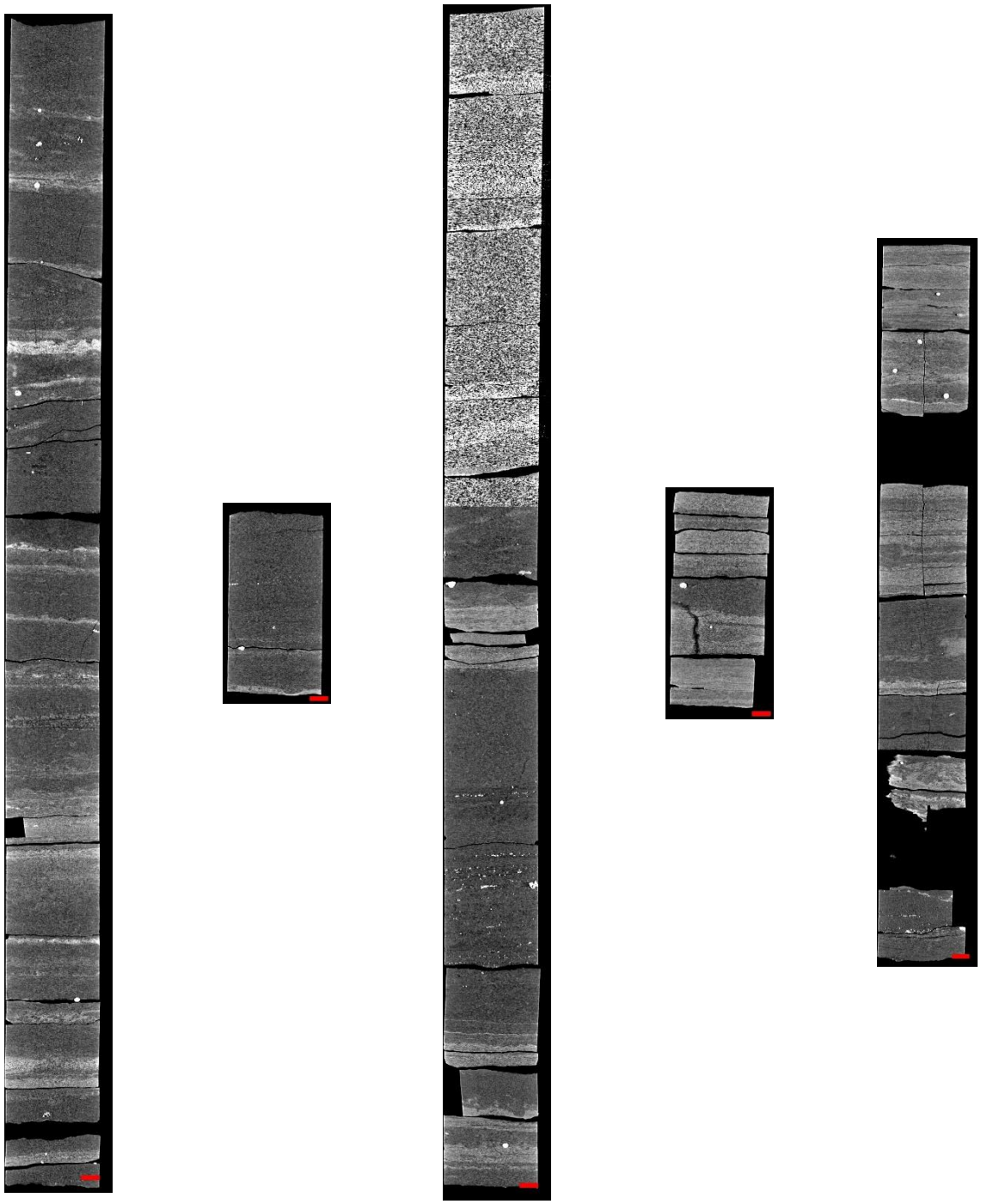

6,156–6,162 ft **6,162–6,163 ft** **6,163–6,167 ft** **6,167–6,168 ft** **6,168–6,171 ft**

Figure 39: 2D isolated planes through the vertical center of the medical CT scans of the Wabash #1 well from 6,156 to 6,171 ft.

3.2 ADDITIONAL CT DATA

Additional CT data can be accessed from NETL's EDX online system using the following link: https://edx.netl.doe.gov/dataset/isgs-seal-wells. The original CT data is available as 16-bit tif stacks suitable for reading with ImageJ (Schneider and Rasband, 2012) or other image analysis software.

3.2.1 Medical CT Image videos

Supplemental to the image videos that display the changes along the cross-sectional, images are also available for download and viewing. A single image from these videos is shown in Figure 40, which showcases a cross section of a heavily bioturbated zone from a depth of 6,139 to 6,144 ft. The red line in the XZ-plane image of the core indicates the location of the XY-plane displayed above (Figure 40). The videos on EDX show this XY variation along the entire length of the core.

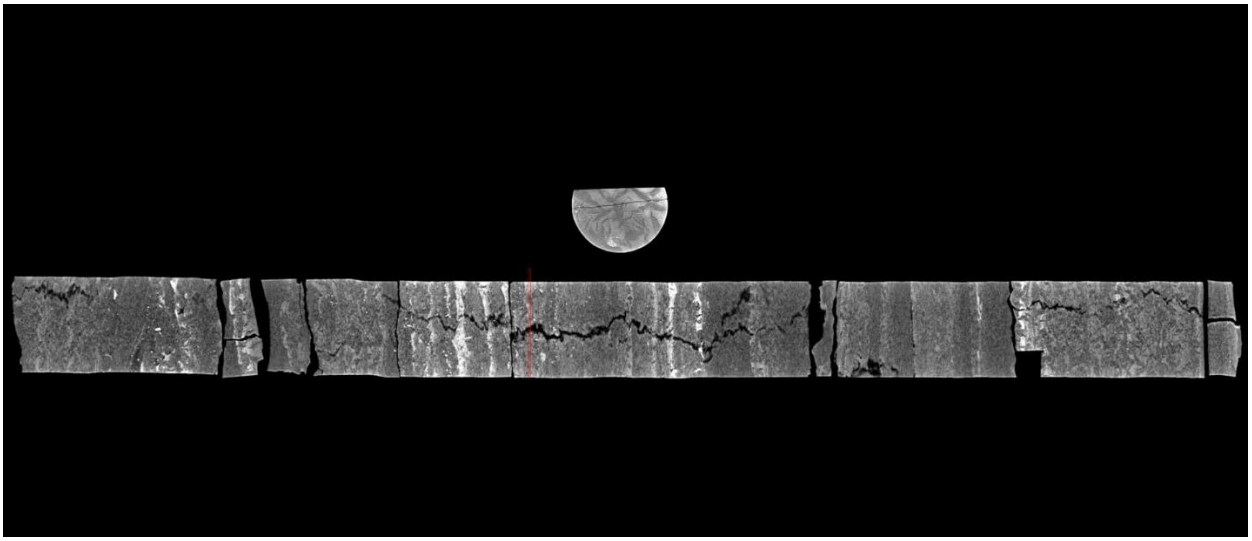

Figure 40: Single image from a video file available on EDX showing variation in the Wabash #1 core from 6,139 to 6,144 ft. The image above shows the variation in composition within the matrix perpendicular to the core length.

3.2.2 Industrial CT Scanning

Detailed scans of a section of interest (see Section 3.4) were performed using the NorthStar Imaging Inc. M-5000® Industrial Computed Tomography System (Industrial CT) at NETL (Figure 41). This system was used to obtain higher resolution scans with variable voxel resolution between 20 and 60 μm^3 (Table 2), allowing for the clear capture of fine details such as fracture spacing and porosity. Examples of these scans can be seen in Figure 42 and Figure 43, with scale bars representing 5 mm. The scans were performed with a voltage of 185 kV and a current of 400 µA or 185 kV and 200 µA for whole cores and smaller diameter sub-cores, respectively, to provide the appropriate photon energy for penetrating the samples. The samples were rotated 360° and 1,440 radiograph projections of the samples were obtained, averaging 12 individual radiographs at each step to create the reconstruction.

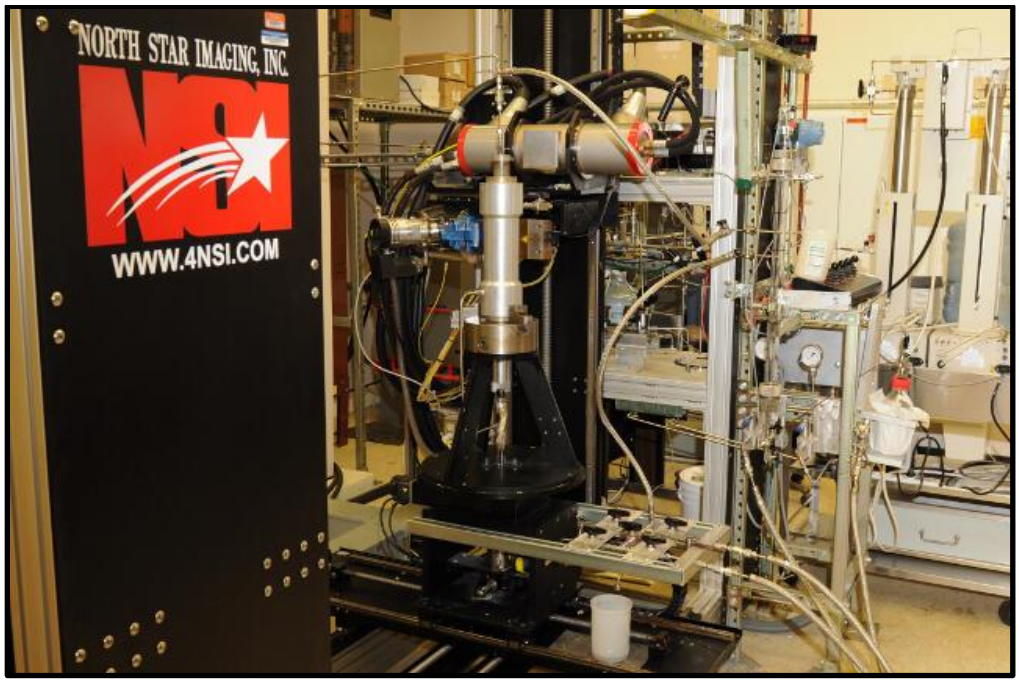

Figure 41: North Star Imaging Inc. M-5000 ® Industrial CT Scanner at NETL used for core analysis.

Table 2: Industrial Scans from Plugs and Whole Core, All Available on EDX

Depth	File Name	Resolution (μm^3)
2,457	EAU_CL_2457_MIC	49.7
2,476	EAU_CL_2476_MIC	49.7
2,602	GM #2_Bx-1_2602_ MIC	60
2,604	GM #2_Bx-1_2604_ MIC	60
2,617.75	GM #2_Bx-4_2617-75_MIC	60
6,107.4	WABASH #1_211_6107-4_ MIC	60
6,115.7	WABASH #1_213_6115-7_MIC	60
6,120	WABASH #1_213_6120_MIC	60
6,123	WABASH #1_213_6123_MIC	60
6,126	WABASH #1_213_6126_MIC	60
6,129	WABASH #1_213_6129 _MIC	60
2,436.6	Viggo_Sub_C-1_Bx-1_2436-6_B_MIC	20
2,437	Viggo_Sub_C-1_Bx-1_2437_A_MIC	20
2,437	Viggo_Sub_C-1_Bx-1_2437_B_MIC	20
5,489	Viggo_Sub_C-1_Bx-32_5489_A_MIC	20
5,489	Viggo_Sub_C-1_Bx-32_5489_B_MIC	20
5,509.2	Viggo_Sub_C-1_Bx-39_5509-2_MIC	20
5,539	Viggo_Sub_C-1_Bx-41_5539_B_MIC	20
5,539	Viggo_Sub_C-1_Bx-41_5539_C_MIC	20
2,481.6	Viggo_Sub_C-1_Bx-9_2481-6_B_MIC	20
6,112.4	Viggo_Sub_C-2_Bx-2_6112-4_B_MIC	20
6,112.4	Viggo_Sub_C-2_Bx-2_6112-4_C_MIC	20
6,115.4	Viggo_Sub_C-2_Bx-2_6115-4_A_MIC	20
6,115.7	Viggo_Sub_C-2_Bx-2_6115-7_A_MIC	20
6,115.7	Viggo_Sub_C-2_Bx-2_6115-7_B_MIC	20
6,117.2	Viggo_Sub_C-2_Bx-3_6117-2_A_MIC	20
6,117.2	Viggo_Sub_C-2_Bx-3_6117-2_B_MIC	20
5,540	VW1_Bx-41_5540_ MIC	60
5,541	VW1_Bx-41_5541_ MIC	60

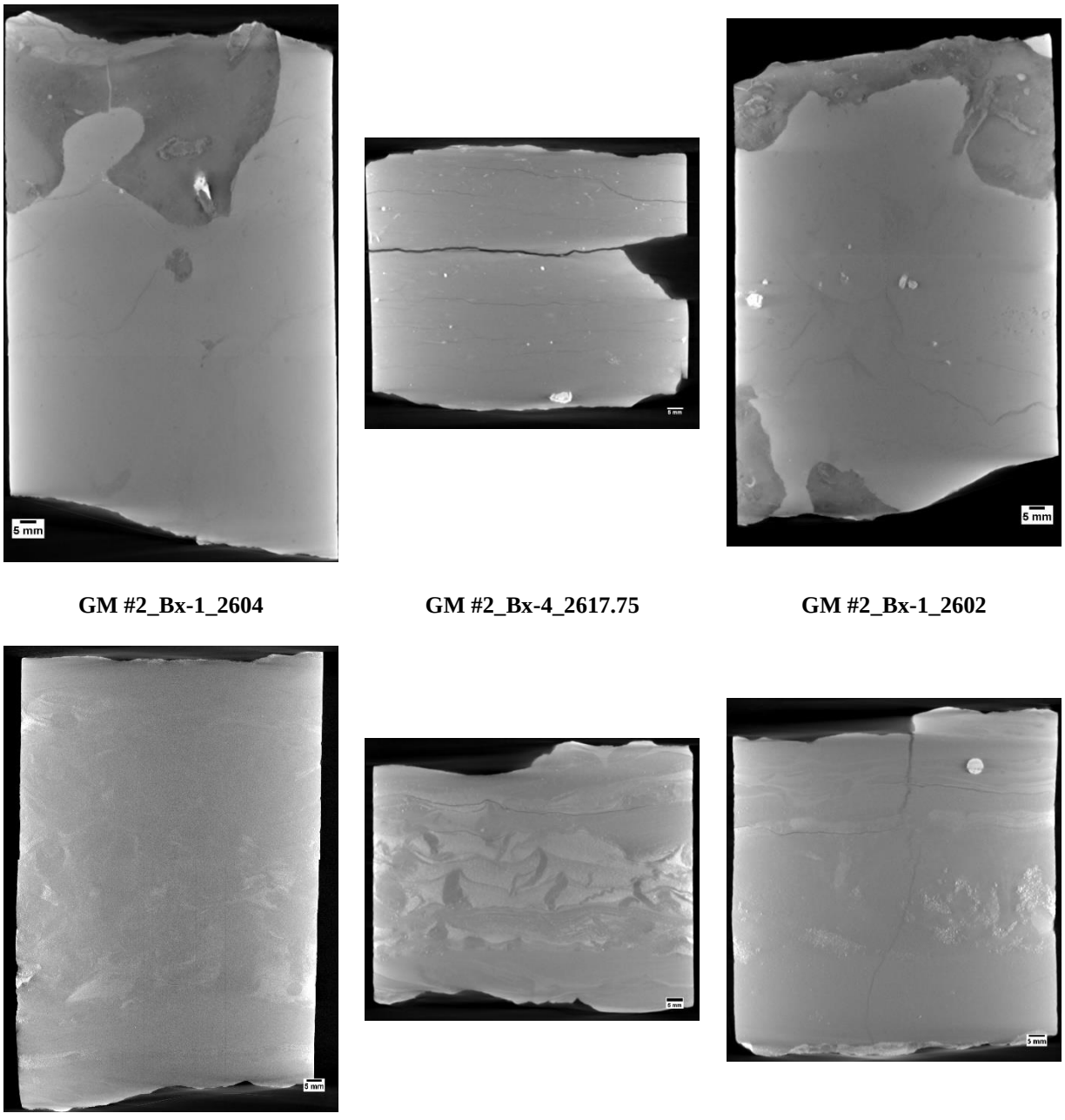

GM #2_Bx-1_2604 **GM #2_Bx-4_2617.75** **GM #2_Bx-1_2602**

Wabash #1_Bx-211_6107.4 **Wabash #1_Bx-213_6115.7** **Wabash #1_Bx-213_6120**

Figure 42: Industrial CT reslices of volumes for GM #2 and Wabash #1 wells, listed in Table 2.

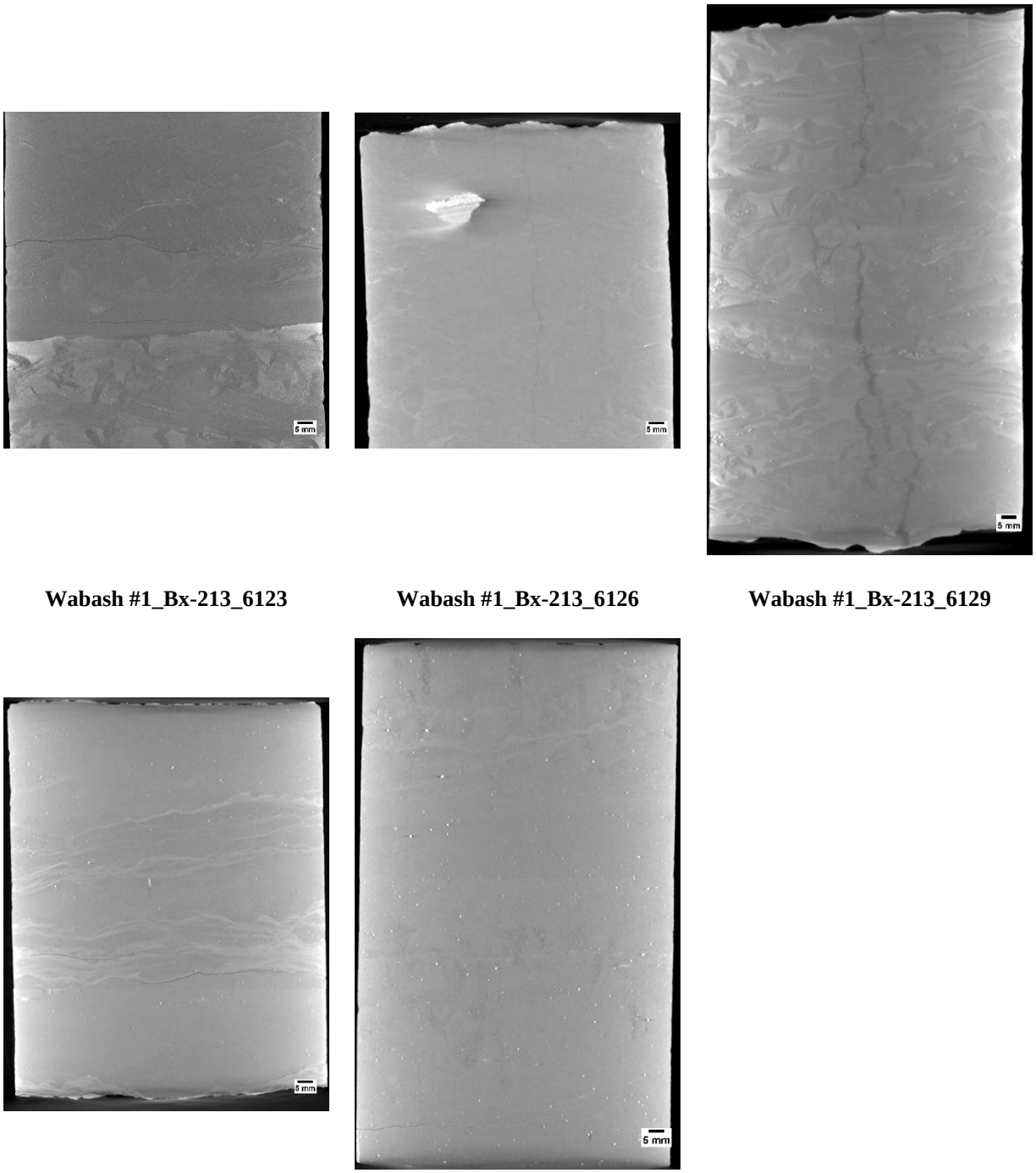

Wabash #1_Bx-213_6123 **Wabash #1_Bx-213_6126** **Wabash #1_Bx-213_6129**

VW1_Box-41_5540 **VW1_Box-41_5541**

Figure 43: Industrial CT reslices of volumes for samples from Wabash #1 and VW #1, listed in Table 2.

3.2.3 Micro-CT scanning

Detailed micro-CT scans of mm-scale sub-cores from select regions of Wabash #1 core were performed at NETL. The micro-CT scanner discussed in Section 2.3 were used to obtain higher resolution images with voxel resolutions at 1.88 μm^3 and capture the details of internal features clearly, e.g., inter-crystalline porosity. A list of the core sections scanned with the micro-CT scanner is shown in Table 3.

Table 3: Micro-CT Scans from Whole Core

Depth	File Name	Resolution (μm^3)
6,116	20220309 Wabash #1 IN 168045_C2B2_6116.0	1.88
4,771	20220504 Wabash #1b Sub C2B2 6110.85	1.88
5,813	20220506 Wabash #1 SEM C2B3 6116.9	1.88

3.3 DUAL ENERGY CT SCANNING

Dual energy CT scanning uses two sets of images, produced at different X-ray energies, to approximate the density (ρ_B) (Siddiqui and Khamees, 2004; Johnson, 2012). The technique relies on the use of several standards of known ρ_B to be scanned at the same energies as the specimen. These scans are performed at lower energies (<100 KeV) and higher energies (>100 KeV) to induce two types of photon interactions with the object (Figure 44). The lower energy scans induce photoelectric absorption, which occurs when the energy of the photon is completely absorbed by the object mass and causes ejection of an outer orbital electron (Figure 44a). The higher energy scans induce Compton scattering, which causes a secondary emission of a lower energy photon due to incomplete absorption of the photon energy in addition to an electron ejection (Figure 44b).

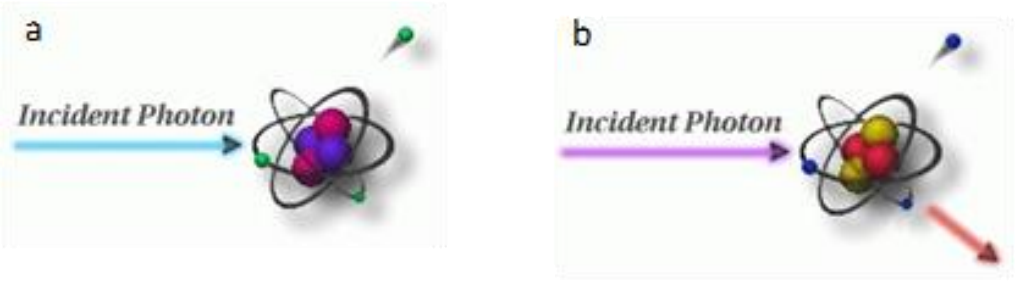

Figure 44: Photon interactions at varying energies. a) Photoelectric absorption, b) Compton scattering. Modified from Iowa State University Center for Nondestructive Evaluation (2021).

Medical grade CT scanners are typically calibrated to known standards, with the output being translated in CTN or Hounsfield Units (HU). Convention for HU defines air as -1000 and water as 0. A linear transform of recorded HU values is performed to convert them into CTN. This study used CTN as it is the native export format for the instrument, but it is possible to use HU. Dual energy CT requires at least three calibration points, and it is prudent to

utilize standards that approximate the object or material of interest. Pure samples of aluminum, graphite, and sodium chloride were used as the calibration standards as they most closely approximate the rocks and minerals of interest (Table 5). Most materials denser than water or with higher atomic masses have a non-linear response to differing CT energies (Table 4).

Table 4: Dual Energy Calibration Standards, Bulk Density (g/cm^3)

Material	ρ_B (g/cm^3)
Air	-0.001
Water	1
Graphite	2.3
Sodium Chloride	2.16
Aluminum	2.7

Table 5: Dual Energy Calibration Standards, HU and CTN for "Low" and "High" Energies

Material	HU		CTN	
	80 KeV	135 KeV	80 KeV	135 KeV
Air	-993	-994	31,775	31,774
Water	-3.56	-2.09	32,764	32,766
Graphite	381	437	33,149	33,205
Sodium Chloride	1,846	1,237	34,614	34,005
Aluminum	2,683	2,025	35,451	34,793

Dual energy CT utilizes these differences to calibrate to the X-ray spectra. Two equations with three unknowns each are utilized to find ρ_B (Siddiqui and Khamees, 2004):

$$\rho_B = mCTN_{low} + pCTN_{high} + q$$

Where [m, p, and q] and [r, s, and t] are unknown coefficients that can be solved by setting up a system of equations with four 3x3 determinants. The CTN is obtained from the CT scans for each of the homogenous calibration standards.

In this study, the high and low energy image stacks were loaded into Python as arrays. A 3D Gaussian blur filter with a sigma of 2 was used to reduce noise in the images. The scipy.solv module of Python was then employed to solve for the coefficients based on the calibration CTN values. The ρ_B was solved for each pixel in the 3D volume and saved as two new separate image stacks.

3.4 COMPILED CORE LOG

The compiled core logs were scaled to fit on single pages for rapid review of the combined data from the medical CT scans and MSCL readings. Logs are presented for each of the three wells including a plot for the Maquoketa shale and Eau Claire shale sections of the Wabash #1 well. Each interval has one image that includes the following tracks expanded in the following paragraphs: track 1, gamma density, and dual energy density (red – averaged using 2-sigma 3D Gaussian Blur, and green – averaged using non-local means denoising); track 2, medical CT images, cropped to center portion of images to highlight grayscale variations; track 3, XRF mineralogy, carbonates (blue; Mg + Ca), quartz (Si), and clays (gray; Al, red; Fe); tracks 4, 5, 6 and 7, elemental proxies; and tracks 8 and 9, elemental ratios.

The elemental results from the XRF were limited to elemental proxies related to skeletal influx/carbonate potential (Ca, Mg, and Mn), detrital influence (Zr, Ti, Al, Si), chalcophiles (Pb, S, Fe), redox potential (Co, Ni, Cu, and V), biogenic production (V*), and Cl to show areas where there may have been inference due to drilling muds (note the areas in red for VW #1).

Trends in elemental ratios can provide insight into mineral composition, oxidation state, and depositional setting. Examples include: Ca/Si, which provides information on relative abundance of calcium carbonates versus silicates; Mn/Fe, which provides information on oxidation, where a decrease in the ratio is related to zones of anoxic/euxinic conditions and an increase is related to zones of dysoxic/oxic conditions; S/Fe, which provides information on the abundance of pyrite (and other iron sulfates) versus Fe oxide minerals; Fe/Al, which provides information into pyrite and iron hydroxide enrichments; Ti/Al, which provides information about terrigenous input; and Si/Al, which provides information on the abundance of illite and micas versus other clays. Magnetic susceptibility can test for iron sulfides (reducing) or oxidized Fe and sulfate. The ratio plot also includes an XRF “mineralogy” with Al, representing clays; Ca, representing calcite; and Si, representing only quartz, although there is some Si contribution to the clays. Pyrite (reduced) should have low magnetic susceptibility; Fe oxide or hydroxide should have high magnetic susceptibility. These broad trends can quickly give information on large suites of core and direct more focused research. These logs are presented in the following images (Figure 45 to Figure 48Figure 48Figure 45: Compiled core log for GM #2 well, Maquoketa and overlying and underlying limestones contacts (Silurian Lime and Galena, respectively) from 2,600 to 2,825 ft. Track 3 header, XRF mineralogy, carbonates (blue, Mg + Ca), quartz (yellow, Si), and clays (gray, Al; red; Fe).).

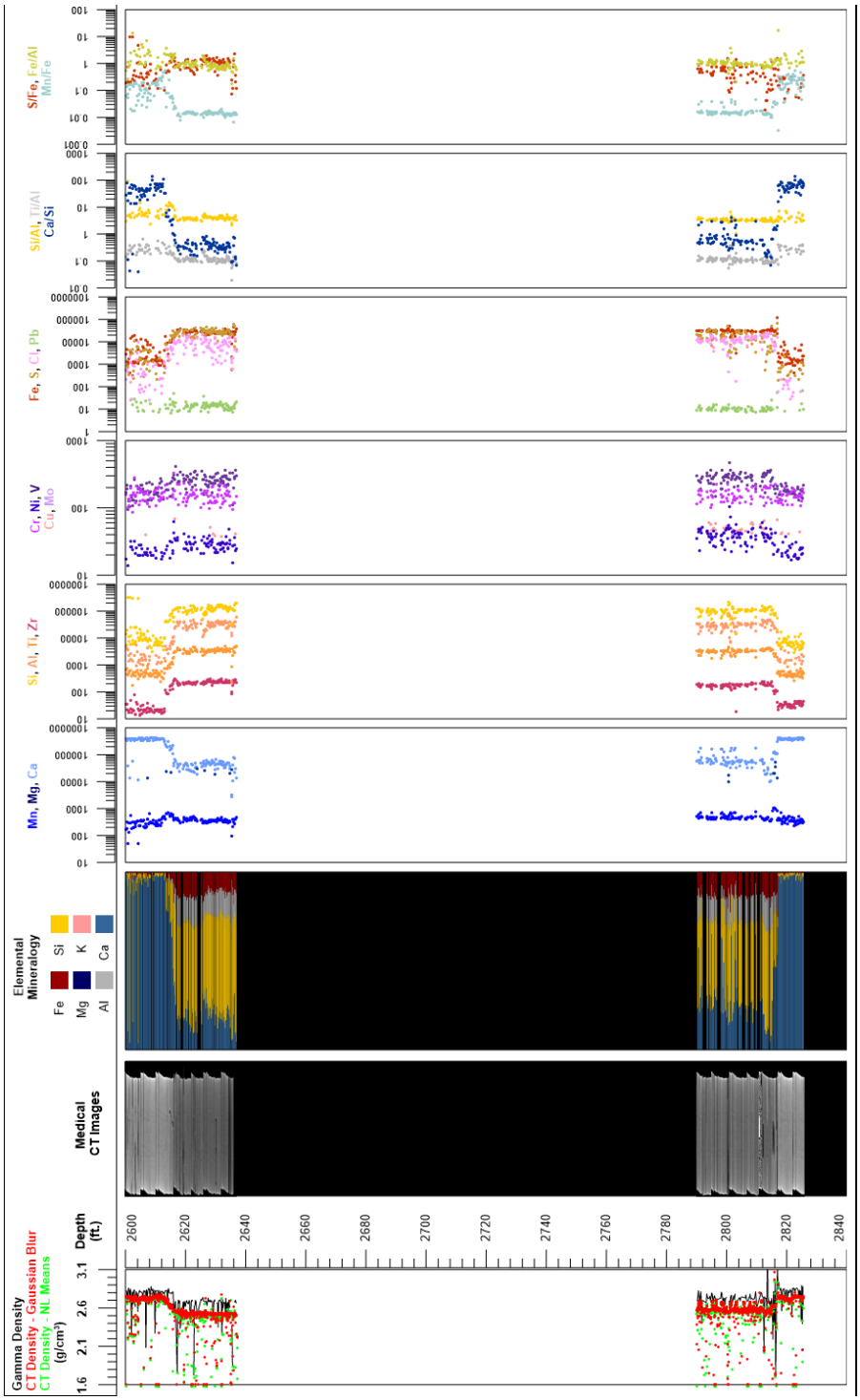

Figure 45: Compiled core log for GM #2 well, Maquoketa and overlying and underlying limestones contacts (Silurian Lime and Galena, respectively) from 2,600 to 2,825 ft. Track 3 header, XRF mineralogy, carbonates (blue, Mg + Ca), quartz (yellow, Si), and clays (gray, Al; red; Fe).

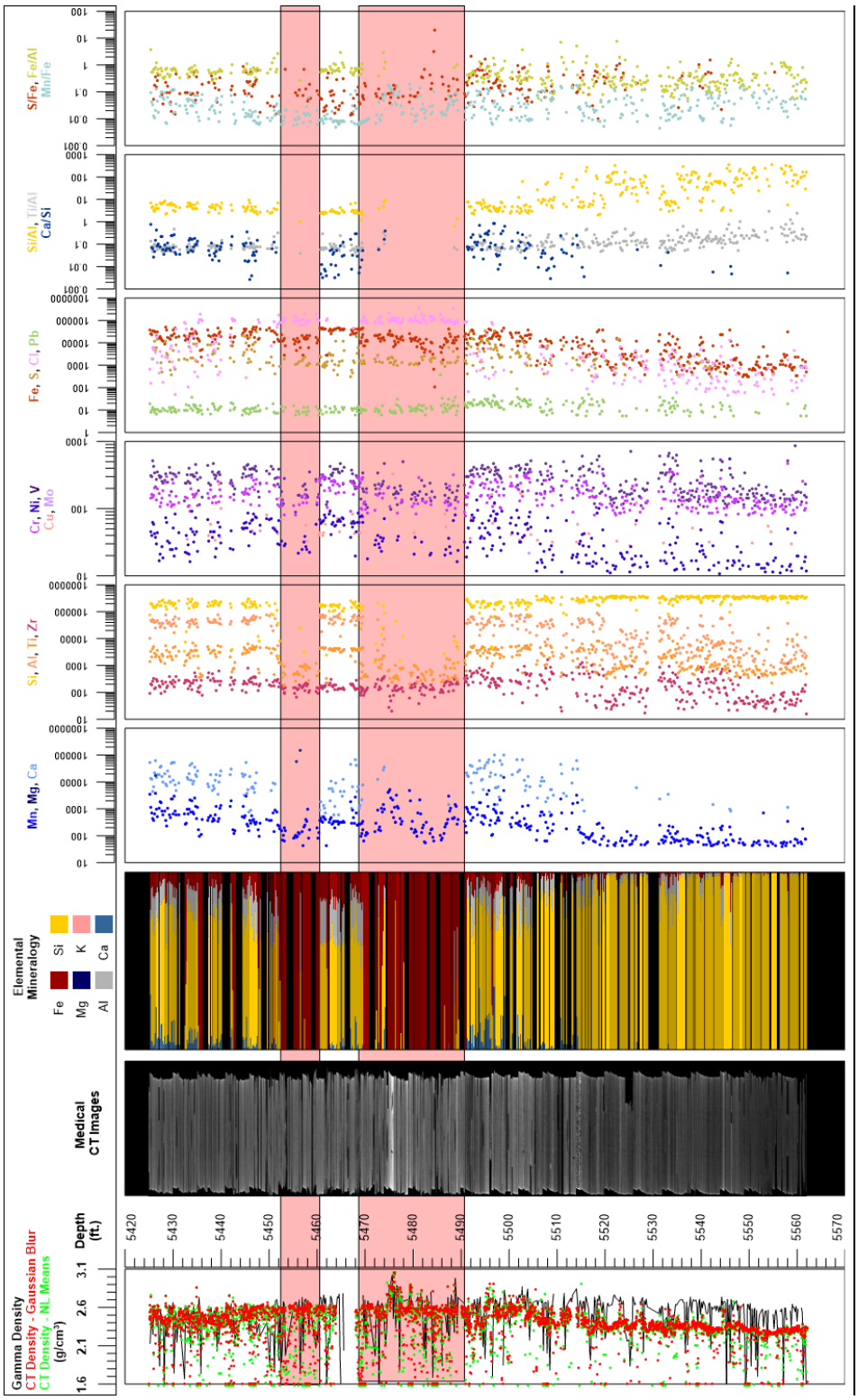

Figure 46: Compiled core log for VW #1 well, Eau Claire from 5,425 to 5,562 ft. Track 3 header, XRF mineralogy, carbonates (blue, Mg + Ca), quartz (yellow, Si), and clays (gray, Al; red, Fe; pink, K).

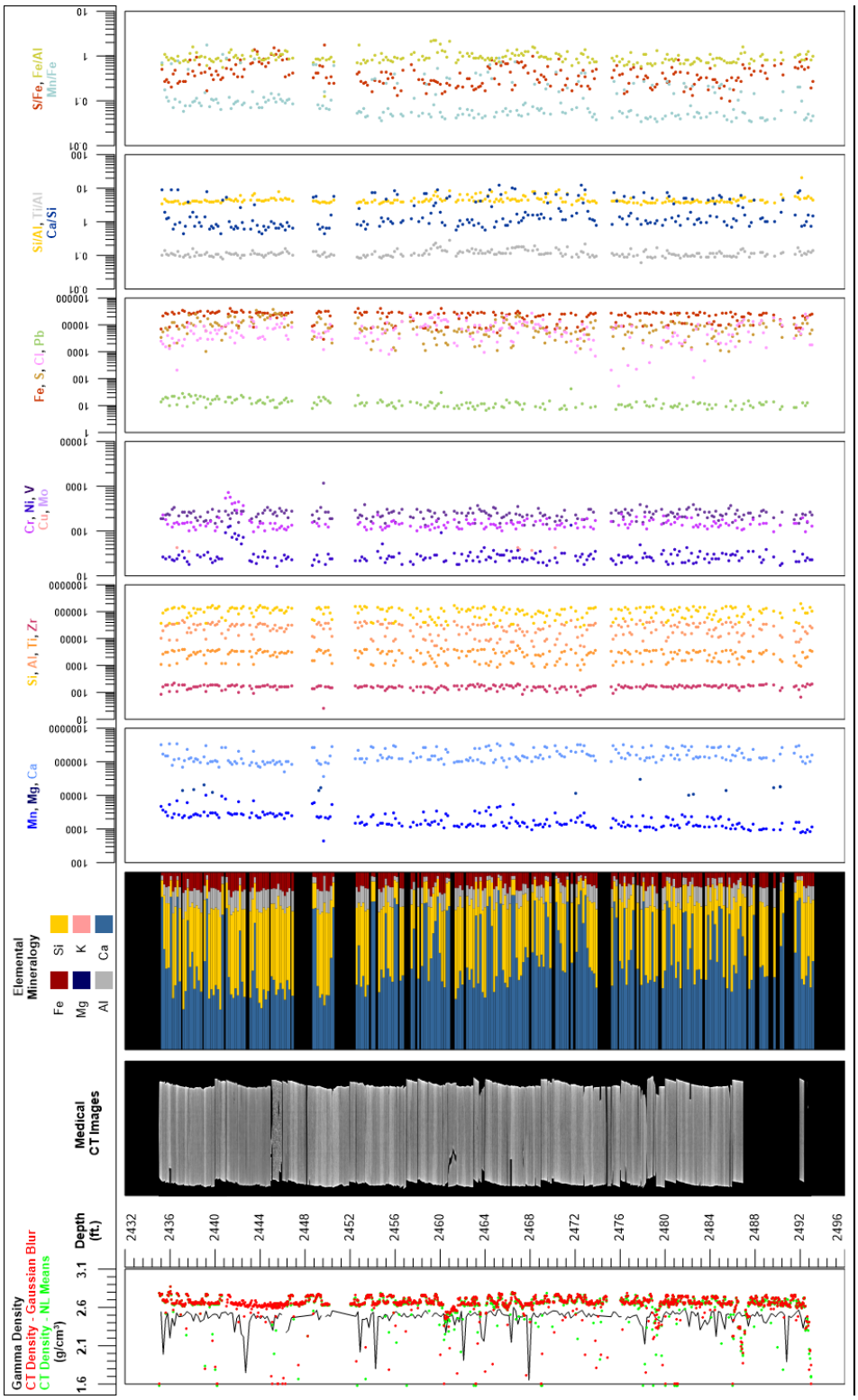

Figure 47: Compiled core log for Wabash #1 well, Maquoketa Formation from 2,435 to 2,493 ft. Track 3 header, XRF mineralogy, carbonates (blue, Mg + Ca), quartz (yellow, Si), and clays (gray, Al; red, Fe; pink, K).

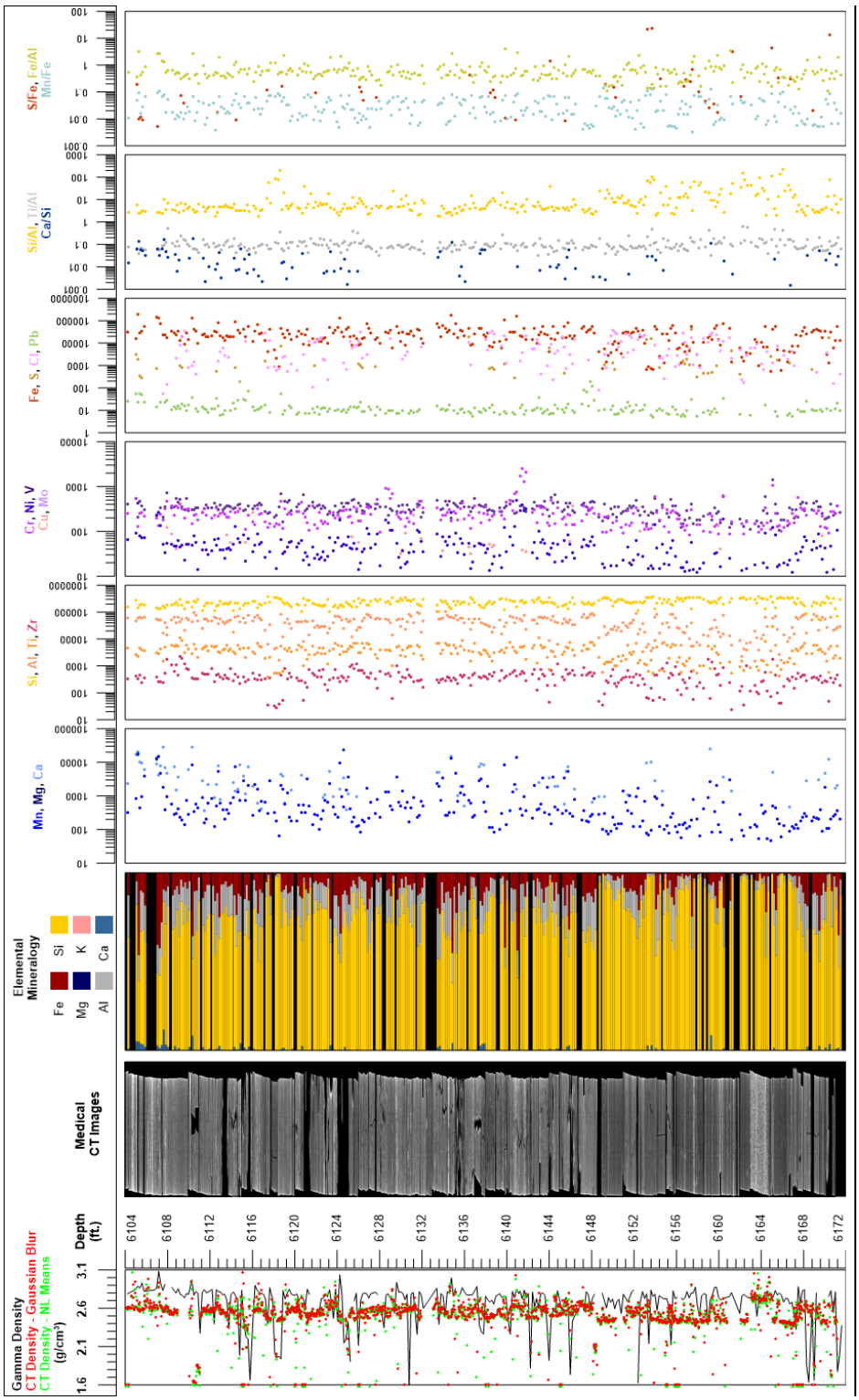

Figure 48: Compiled core log for Wabash #1 well, Eau Claire Formation from 6,104 to 6,171.5 ft. Track 3 header, XRF mineralogy, carbonates (blue, Mg + Ca), quartz (yellow, Si), and clays (gray, Al; red, Fe; pink, K).

4. DISCUSSION

The evaluation of the magnetic susceptibility, P-wave velocity, XRF, and CT analysis offers a unique look into the internal structure of the core and macroscopic changes in lithology. These methods:

- Are non-destructive.
- Offer a more thorough understanding of the core when employed together than any single technique alone.
- Can be used to identify zones of interest for further detailed analysis, experimentation, and quantification.
- Provide a detailed digital record of the core, before any destructive testing or further degradation, that is accessible and can be referenced for future studies.

5. REFERENCES

Bauer, R. A.; Will, R.; Greenberg, S. E.; Whittaker, S.G. Illinois Basin–Decatur project. *Geophysics and Geosequestration;* Cambridge University Press, 2019; pp. 339–369.

Blakley, C.; Carman, C.; Monson, C.; Freiburg, J.; Korose, C. *Developing CO_2 Source and Storage Opportunities across the Illinois Basin Subtask 5.3–Regional Roadmap for Source Network and Storage Deployment Topical Report*; No. DOE/FE002945-8; Univ. of Illinois at Urbana-Champaign, IL, 2019.

Crandall, D.; Moore, J.; Rodriguez, R.; Gill, M.; Soeder, D.; McIntyre, D.; Brown, S. *Characterization of Martinsburg Formation using Computed Tomography and Geophysical Logging Techniques*; NETL-TRS-4-2017; NETL Technical Report Series; U.S. Department of Energy, National Energy Technology Laboratory: Morgantown, WV, 2017; p 68.

Energy.gov. Project Descriptions: Coal FIRST Initiative Invests $80 Million in Net-Zero Carbon Electricity and Hydrogen Plants, 2020. https://www.energy.gov/fe/project-descriptions-coal-first-initiative-invests-80-million-net-zero-carbon-electricity-and. (accessed Aug 23, 2021).

Geotek Ltd. Geotek Multi-Sensor Core Logger Flyer, Daventry, UK, 2009. http://www.geotek.co.uk/sites/default/files/MSCLOverview.pdf

Geotek Ltd. Multi-Sensor Core Logger Manual; Version 05-10; Published by Geotek, 3 Faraday Close, Daventry, Northamptonshire NN11 8RD, 2010. info@geotek.co.uk, www.geotek.co.uk

Hunts, C.; Moskowitz, B.; Banerjee, S. *Magnetic Properties of Rocks and Minerals;* Rock Physics and Phase Relations: A Handbook of Physical Constants; 1995, 3; p 189–204.

Iowa State University Center for Nondestructive Evaluation, Ames, IA, 2021. https://www.nde-ed.org/Physics/X-Ray/attenuation.xhtml (accessed July 2021).

ISGS. Wabash CarbonSAFE Well Information. Illinois State Geological Survey (ISGS), 2022.

Johnson, T. R. C. Dual-Energy CT: General Principles. *American Journal of Roentgenology* **2012,** *199*, S3–S8. DOI: 10.2214/AJR.12.9116.

Korose, C.; Whittaker, S. Wabash CarbonSAFE DE-FE0031626; Carbon Storage Project Review Meeting; U.S. Department of Energy; National Energy Technology Laboratory; 2020.

Paronish, T.; Schmitt, R.; Crandall, D.; Moore, J.; Carman, C. H.; Freiburg, J. T.; Whittaker, S.; Korose, C. P. *Computed Tomography Scanning and Geophysical Measurements of the Wabash No.1 Core*; DOE.NETL-2021.2656; NETL Technical Report Series; U.S. Department of Energy, National Energy Technology Laboratory: Morgantown, WV, 2021; p 40. https://edx.netl.doe.gov/dataset/computed-tomography-scanning-and-geophysical-measurements-of-the-wabash-no-1-core. DOI: 10.2172/1819826.

Rasband, W. S. *ImageJ*. U.S. National Institutes of Health: Bethesda, MD, 1997–2019, http://imagej.nih.gov/ij/ (accessed 2019).

Schneider, C. A.; Rasband, W. S.; Eliceiri, K. W. NIH Image to ImageJ: 25 years of image analysis. *Nature Methods* **2012,** *9*, 671–675.

Siddiqui, S.; Khamees, A. A. Dual-Energy CT-Scanning Applications in Rock Characterization. *Society of Petroleum Engineers* **2004**. DOI:10.2118/90520-MS.

Wabash Valley Resources, West Terre Haute, IN, 2021. https://www.wvresc.com/doe-80million/ (accessed January 2023).

Brian Anderson
Director
National Energy Technology Laboratory
U.S. Department of Energy

David Alleman
Associate Director
Office of Research & Development
(FE-32)
U.S. Department of Energy

John Wimer
Acting Chief Research Officer
Science & Technology Strategic Plans
& Programs
National Energy Technology Laboratory
U.S. Department of Energy

Bryan Morreale
Associate Laboratory Director for
Research & Innovation
Research & Innovation Center
National Energy Technology Laboratory
U.S. Department of Energy

NETL Technical Report Series